NOAA OAR Special Report

PMEL Tsunami Forecast Series: Vol. #
A Tsunami Forecast Model for Keauhou, Hawaii

(Draft)

Liujuan Tang

August 2011

NOAA Center for Tsunami Research (NCTR)
Pacific Marine Environmental Laboratory

Contents

List of Tables

PMEL Tsunami Forecast Series: Vol.
A Tsunami Forecast Model for Keauhou, Hawaii

Liujuan Tang

Abstract

This study describes the development, validation, and testing of a tsunami forecast model for Keauhou, Hawaii. Based on the Method of Splitting Tsunamis (MOST) model, the forecast model is capable of simulating four hours of tsunami wave dynamics at a resolution of 1-arc-sec (~30 m) in minutes of computational time. A reference inundation model of higher resolution of 1/3 arc-sec (~10 m) was also developed in parallel, to provide modeling references for the forecast model. Both models were tested for seventeen past tsunamis and a set of eighteen simulated magnitude 9.3 tsunamis.

The numerical consistency between the model outputs on the amplitude time series at warning point, maximum amplitude and current in the forecast area, are good in general. The difference in the maximum amplitude at the warning point between the reference and forecast models is within 17 cm when it is under 1 m (except the 1946 tsunami, which shows a 31 cm difference for a maximum amplitude of 65 cm), and less than 20% when it is greater than 1 m (except the magnitude 9.3 tsunamis from Central Aleutian, Kamchatka and Izu subdection zones, from which the difference can be 33%).

The simulated magnitude 9.3 tsunamis show an impressive local variability of tsunami amplitudes at Keauhou, and indicate the complexity of forecasting tsunami amplitudes at a coastal location. It is essential to use high-resolution models in order to provide accuracy that is useful for coastal tsunami forecast for practical guidance.

The study highlight tsunamis from Japan, Kamchatka, Northern Tonga (Samoa), Isu, Southern Chile, and East Philippines and Central Aleutian subduction zones can potentially generate large amplitude waves in Keauhou. It also shows the water front at Kahaluu Beach Park and at end of Keauhou bay are under high flooding risk once inundation occurs in the forecast area.

1 Background and Objective

The National Oceanic and Atmospheric Administration (NOAA) Center for Tsunami Research at NOAA's Pacific Marine Environmental Laboratory (PMEL) has developed a tsunami forecasting system for operational use by NOAA's two Tsunami Warning Centers located in Hawaii and Alaska (Titov et al., 2005; Titov, 2009). The forecast system combines real-time deep-ocean tsunami measurements from Deep-ocean Assessment and Reporting of Tsunami (DART) buoys (*Gonzalez et al*., 2005; *Bernard et*

al., 2006, *Bernard and Titov*, 2007) with the Method of Splitting Tsunami (MOST) model, a suite of finite difference numerical codes based on nonlinear long wave approximation (*Titov and Synolakis*, 1998; *Titov and Gonzalez*, 1997; *Synolakis*, *et al*., 2008) to produce real-time forecasts of tsunami arrival time, heights, periods and inundation. To achieve accurate and detailed forecast of tsunami impact for specific sites, high-resolution tsunami forecast models are under development for United States coastal communities at risk (Tang *et al.*, 2008[a]; 2009[a]). The resolution of these models has to be high enough to resolve the dynamics of a tsunami inside a particular harbor, including influences of major harbor structures such as breakwaters. These models have been integrated as crucial components into the forecast system.

Presently, a system of 41 DART buoys (32 U.S.-, 1 Russian-,1 Chilean-, and 6 Australian- owned) is monitoring tsunami activity in the Pacific Ocean as shown in Figure 1. Globally, the network consists of 52 tsunameters, and deployed in the Atlantic Ocean, the Pacific Ocean, Caribbean and the Gulf of Mexico. The precomputed propagation models currently have 1,106 scenarios to cover Pacific tsunami sources (1,691 globally), and the high-resolution forecast inundation models are now set up for 43 U.S. coastal communities. The fully implemented system will use real-time data from the DART network to provide high-resolution tsunami forecasts for at least 75 communities in the U.S. by 2013 (Titov, 2009). Since its first testing in the 17 November 2003 Rat Island tsunami, the forecast system has produced experimental realt-ime forecasts for 17 tsunamis in the Pacific and Indian oceans (Titov et al., 2005; Wei et al., 2008; Titov, 2009; Tang et al., 2011). The forecast methodology has also been tested with the data from nine additional events that produced the deep-ocean data.

Two recent tsunamis, the 2009 Samoa and 2011 Japan tsunamis caused flooding and damaging in the Kahaluu-Keauhou area, highlighting the need of a forecast flooding model for this area. The report describes the development, testing and applications of the Keauhou forecast model. The objective is to provide NOAA's Tsunami Warning Centers the ability to assess danger posed to Keauhou following tsunami generation in the Pacific Ocean Basin, and to provide accurate and timely forecasts to enable the community to respond appropriately. A secondary objective is to explore the potential tsunami impact from earthquakes at major subduction zones in Pacific to the site by using the developed flooding model.

The report is organized as follows. Section 2 briefly introduces NOAA's tsunami forecast methodology. Section 3 describes the model development. Section 4 presents the results and discussion, which includes sensitivity of the forecast model to model setup, verification, and testing for past and simulated tsunamis. A summary and conclusion are provided in section 5.

2 Forecast Methodology

NOAA's real-time tsunami forecasting scheme is a process that comprises of two steps: (1) construction of a tsunami source via inversion of deep ocean DART observations with pre-computed tsunami source functions; and (2) coastal predictions by running high-resolution forecast models in real time (*Titov et al*., 1999; *Titov et al*., 2005; Tang *et al*., 2009[a]). The DART-constrained tsunami source, the corresponding offshore scenario from the tsunami source function database, and high-resolution forecast models cover the entire evolution of earthquake-generated tsunamis, generation, propagation and coastal inundation, providing a complete tsunami forecast capability.

2.1 Construction of A Tsunami Source Based on DART Observations and Tsunami Source Functions

Several real-time data sources, including seismic data, coastal tide gage and deep-ocean data have been used for tsunami warning and forecast (*Satake et al*., 2008; *Whitmore*, 2003; *Titov,* 2009). NOAA's strategy for the real-time forecasting is to use deep-ocean measurements at DART buoys as the primary data source due to several key features. (1) The buoys provide a direct measure of tsunami waves, unlike seismic data, which are an indirect measure of tsunamis. (2) The deep ocean tsunami measurements are in general the earliest tsunami information available, since tsunamis propagate much faster in deep ocean than in shallow coastal area where coastal tide gages are used for tsunami measurements. (3) Compared to coastal tide gages, DART data with a high signal to noise ratio can be obtained without interference from harbor and local shelf effects. (4) Wave dynamics of tsunami propagation in deep ocean is assumed to be linear (Liu, 2009). This linear process allows application of efficient inversion schemes.

Time series of tsunami observations in deep-ocean can be decomposed into a linear combination of a set of tsunami source functions in the time domain by a linear least squares method. We call coefficients obtained through this inversion process *tsunami source coefficients*. The magnitude computed from the sum of the moment of tsunami source functions multiplied by the corresponding coefficients is referred as the *tsunami moment magnitude* (T_{Mw}), to distinguish from the seismic moment magnitude M_w, which is the magnitude of the associated earthquake source. While the seismic and tsunami sources are in general not the same, this approach provides a link between the seismically-derived earthquake magnitude and the tsunami observation-derived tsunami magnitude.

During real-time tsunami forecast, seismic waves propagate much faster than tsunami waves so the initial seismic magnitude can be estimated before the DART measurements are available. Since time is of the essence, the initial tsunami forecast is based on the seismic magnitude only. The T_{Mw} will update the forecast when it is available via DART inversion using the tsunami source function database.

Titov et al.(1999; 2001) conducted sensitivity studies on far-field deep-water tsunamis to different parameters of elastic deformation model described in *Gusiakov* (1978) and *Okada* (1985). The results showed source magnitude and location essentially define far-field tsunami signals for a wide range of subduction zone earthquakes. Other

parameters have secondary influence and can be pre-defined during forecast. Based on these results, tsunami source function databases for Pacific, Atlantic, and Indian Oceans have been built using pre-defined source parameters, length = 100 km, width = 50 km, slip = 1 m, rake = 90 and rigidity = 4.5 x 10^{10} N/m^2. Other parameters are location-specific; details of the databases are described in *Gica et al*. (2008). Each tsunami source function is equivalent to a tsunami from a typical M_w = 7.5 earthquake with defined source parameters. Figure 1 shows the locations of tsunami source functions in Pacific Ocean.

The database can provide offshore forecast of tsunami amplitudes and all other wave parameters immediately once the inversion is complete. The tsunami source, which combines real-time tsunami measurements with tsunami source functions, provides an accurate offshore tsunami scenario without additional time-consuming model runs.

2.2 Real-time Coastal Predictions by High-Resolution Forecast Models.

High-resolution forecast models are designed for the final stage of the evolution of tsunami waves: coastal runup and inundation. Once the DART-constrained tsunami source is obtained (as a linear combination of tsunami source functions), the pre-computed time series of offshore wave height and depth-averaged velocity from the model propagation scenario are applied as the dynamic boundary conditions for the forecast models. This saves the simulation time of basin wide tsunami propagation. Tsunami inundation is a highly nonlinear process, therefore a linear combination would not, in general, provide accurate solutions. A high-resolution model is also required to resolve shorter tsunami wavelengths nearshore with accurate bathymetric/topographic data. The forecast models are constructed with the Method of Splitting Tsunami (MOST) model, a finite difference tsunami inundation model based on nonlinear shallow-water wave equations (*Titov and Gonzalez,* 1997). Each forecast model contains three telescoping computational grids with increasing resolution, covering regional, intermediate and nearshore areas. Runup and inundation are computed at the coastline. For example, Figure 2 shows forecast model setup for several tsunami forecast models in Hawaii, detailing the telescoping grids used:

(a) One regional grid of 2-arc-minute (~3600m) resolution covers the main Hawaiian Islands (Fig. 2.a).

(b) Then the Hawaiian Islands are divided into four intermediate grids of 12- to 18-arc-second (~ 360 –540m) for four natural geographic areas (Figs. 2.b 1-4):

(b1) Ni'ihau, Ka'ula Rock, and Kauai (Kauai complex),

(b2) Oahu,

(b3) Molokai, Maui, Lanai, and Kaho'olawe (the Maui Complex),

(b4) Hawaii.

(c) Each intermediate grid contains 2-arc-second (~60 m) nearshore grids (Figs. 2.c 1-4).

The highest resolution grid includes the population center and tide stations for forecast verification. The grids are derived from the best available bathymetric/topographic data at the time of development, and will be updated as new survey data become available.

The forecast models are optimized for speed and accuracy. By reducing the computational areas and grid resolutions, each model is optimized to provide 4-hour event forecasting results in minutes of computational time using one single processor, while still providing good accuracy for forecasting. To ensure forecast accuracy at every step of the process, the model outputs are validated with historical tsunami records and compared to numerical results from a reference inundation model with higher resolutions and larger computational domains. In order to provide warning guidance for long duration during a tsunami event, each forecast model has been tested to output up to 24-hour simulation since tsunami generation.

3 Model Development

3.1 Forecast area

The main Hawaiian Islands are the younger and southern portion of the Hawaii Archipelago. From northwest to southeast, the islands form four natural geographic groups by shared channels and inter-island shelf, including (1) Ni'ihau, Ka'ula Rock, and Kauai, (Kauai complex) (2) Oahu, (3) Molokai, Maui, Lanai, and Kaho'olawe, (the Maui Complex), and (4) Hawaii. Kahaluu-Keauhou is located at the southwest shore of the Big Island of Hawaii. As of the 2010 Census, it had a resident population of 3549 and 1457 households. Figure 3 presents an aerial photo of this area and a chart is shown in Figure 4. The population density data is in Figure 5.

The Island of Hawaii (Big Island) locates at the southeast end of the Hawaii Archipelago (Fig. 2). To its northwest, there is the Maui complex, with the deep Alenuihaha Channel in between (water depth greater 200m). Gentle slope from 0 to 100 m water depth followed by sudden steep offshore slopes from 100m down to 4000 m depth feature the coast of Kahaluu-Keauhou area. From 0 to 100m depth, the slope is quite gentle, only 0.013. From 100m to 1000m water depth, it is the steepest offshore slope of 0.3822, and then 0.15 slope from 1000m to 4000m depth.

No tide station exists in the forecast area. The Kawaihae tide station on the same west coast of the Island, which is approximately 53 km to the north, is the closest station to this area. At Kawaihae station, the mean range of tide is 0.461m, and the Mean High Water is 0.222 m above Mean Sea Level. Since no tide gage is in the area, a point (204.03740740°E, 19.5616666 ° N) at 3.6m water depth near the end of Keauhou bay was chosen as the warning point (Fig. 7d).

3.2 Tsunami history and data

Hawaii Islands had a long history of distance and local destructive tsunamis (Pararas-Carayannis, 1969; Soloviev and Go, 1984; Lander and Lockridge, 1989). The descriptions for Keauhou were extracted from the references as follows. The height in Pararas-Carayannis (1969) refers to maximum runup height or amplitude. Walker (2004) summarized the runups on the Island of Hawaii for the 1946, 1952, 1957, 1960 and 1964 tsunamis (Figure 5).

The earliest recorded tsunami damage at Keauhou was on April 3, 1868, when a magnitude 7-7.5 earthquake occurred in S.E. Hawaii. "Right after the quake ended, the sea inundated a to the two basaltic columns on the road to Keauhou; all buildings were swept away" (Pararas-Carayannis, 1969).

On June 15, 1896, a tsunami originated from Sanriku, Japan produced a 9.1 m height at Keauhou (Pararas-Carayannis, 1969).

On August 9,1901, a tsunami originated from Rikuchu, Japan swept a house away at Keauhou. Kailua was flooded. No disturbance was noticed elsewhere in the Hawaiian Islands (Pararas-Carayannis, 1969).

On April 1, 1946, a 4 m height was observed for the Unimak tsunami (Pararas-Carayannis, 1969).

On March 17, 1952, a tsunami originated from Hokkaido, Japan produced a 0.9 m height at Keauhou (Pararas-Carayannis, 1969).

On March 9, 1957, a 2.1m height was observed at Keauhou for the Andreanof Island tsunami (Pararas-Carayannis, 1969).

On May 22, 1960, a 3.7 m height was observed at Keauhou for the Chile tsunami(Pararas-Carayannis, 1969).

On September 29, 2009, the Samoa tsunami flooded the Parking area near the Keauhou Boat Ramp.

On March 11 2011, the Japan tsunami hit Keauhou bay hard. Water slammed into the end of the Keauhou bay, destroying Keauhou Yacht Club and severely damaging three ocean sports activity offices (Bracken, 2011). "Well into the day on Friday, surges continued to sweep over the road, invade nearby structures and throw fish far back up onto land" (Rizzuto, 2011). The Keauhou Boat Ramp and Keauhou Pier were also damaged. The Kahalulu Beach Park was flooding, with rocks and debris left everywhere. The water also undermined a small pavilion when waves crashed over the top (Bracken, 2011).

As an area that has repeatedly been damaged and flooded by tsunamis, Keauhou is in need of a forecast model to aid site-specific evacuation decisions.

3.3 Bathymetry and Topography

Tsunami inundation modeling requires accurate bathymetry in coastal area as well as high resolution topography and bathymetry in the nearshore area. Two gridded digital elevation models (DEMs), one at medium resolution (6 arc-second) for Hawaiian Islands and a high resolution (1/3 arc-second) DEM for Keauhou were developed.

3.3.1 Hawaiian DEM in 6-arc-sec resolution

The 6" Hawaiian DEM was developed at NOAA center for tsunami research in 2007. The same grid has been used for the forecast model developments for Hilo, Kahului, Honolulu, Pearl Harbor and Lahaina (Tang et al, 2009; 2010). The grid was compiled from several data sources; Figure 7a is an overview of the spatial extents of each data source used. In areas where multiple datasets overlapped, higher-resolution and newer datasets were generally preferred, and superseded datasets were used for comparison and verification. An overview of the data sources used was as followed; in general, the data sources listed first superseded data sources listed later when they overlapped.

Source details for the datasets incorporated into the model grids:

- Joint Airborne Lidar Bathymetry Technical Center of Expertise (JALBTCX), US Army Corps of Engineers, Mobile District. Online reference: http://shoals.sam.usace.army.mil/hawaii/pages/Hawaii_Data.htm.
- Monterey Bay Aquarium Research Institute (MBARI) Hawaii Multibeam Survey, Version 1. Online reference: http://www.mbari.org/data/mapping/hawaii/.
- USGS Pacific Seafloor Mapping Project. Online reference: http://walrus.wr.usgs.gov/pacmaps/data.html.
- Japan Agency for Marine-Earth Science and Technology (JAMSTEC) 1998-1999 multibeam bathymetric surveys. Published in: Takahashi, E., *et al*., eds. (2002): *Hawaiian Volcanoes: Deep Underwater Perspectives*. American Geophysical Union Monograph 128.
  JAMSTEC trackline data was recorded by the R/V *Mirai* during transits near in 1999 and 2002. Online reference: http://www.jamstec.go.jp/mirai/index_eng.html.
- United States Army Corps of Engineers (USACE), Honolulu District. Online reference: http://www.poh.usace.army.mil/.
- NOAA National Geophysical Data Center (NGDC). Online reference: http://www.ngdc.noaa.gov/mgg/gdas/gd_sys.html.
- NOAA National Ocean Service (NOS). Sounding points were digitized from NOS nautical charts 19347, 19358, 19359, 19364, 19366, 19342, 19381, and 19324. Sounding data from electronic chart (ENC) 19357 was used. This data was included in relatively shallow regions where other data sources were sparse or unavailable, or for quality control of other sources.

- Smith, W. H. F., and D. T. Sandwell, Global seafloor topography from satellite altimetry and ship depth soundings, *Science*, v. 277, p. 1957-1962, 26 Sept., 1997. Online reference: http://topex.ucsd.edu/WWW_html/mar_topo.html.
- USGS Geological Long-Range Inclined Asdic (GLORIA) surveys. Online data reference: http://walrus.wr.usgs.gov/infobank/
- NOAA Coastal Services Center. http://www.csc.noaa.gov/. The IfSAR topographic data was collected and processed for CSC by Intermap Technologies Inc. The data is subject to a restrictive license agreement and is not publicly available.
- USGS National Elevation Dataset. Online reference: http://seamless.usgs.gov/

The SHOALS LIDAR project, which provides high-resolution unified topographic and bathymetric data around for nearshore areas of several Hawaiian Islands, including all of Maui, was essential to accurate modeling of reef and intertidal regions where conventional bathymetric survey data is usually coarse or unavailable. Quality data in this region is especially essential because bathymetric inaccuracies have great impact on tsunami wave dynamics in shallow water. The 2005 NOAA CSC IfSAR survey of Maui provided similarly valuable high-resolution topography for the entire island, enabling greater confidence in predicting inundation extents. The USGS National Elevation Dataset (NED) was used on other islands outside of the primary study area.

High-resolution gridded datasets derived from multibeam surveys are available for many parts of the archipelago, and were used wherever available. In deep water where high-resolution multibeam data were not available, the grid was developed by interpolation of a combination of USGS GLORIA surveys and the Smith and Sandwell two-minute global seafloor dataset.

All selected input datasets were converted to the mean high water (MHW) vertical datum, as necessary. Bathymetry datasets were converted from the survey tidal datum (usually MLLW or MSL) using offset surfaces interpolated from NOS tide gauges at Kahului, Kawaihae (Hawaii), and Kaunakakai (Molokai). The CSC IfSAR topographic data as obtained was vertically referenced to the GRS80 ellipsoid. It was converted to MHW using an offset surface interpolated from seven National Geodetic Survey (NGS) benchmark stations on Maui that had ellipsoid and tidal heights recorded.

Raw data sources were imported to ESRI ArcGIS-compatible file formats. Horizontal positions were reprojected, where necessary, to the WGS84 horizontal geodetic datum using ArcGIS. In the point datasets, single sounding points that differed substantially from neighboring data were removed. Gridded datasets were checked for extreme values by examination of contour lines, and, where available, by comparison between multiple data sources.

To compile the multiple data sources into a single grid, subsets of the source data were created in the priority order described above. A triangulated irregular network (TIN) was created from the detided vector point data (geodas, usace, csc_lidar). Also added to the TIN were points taken from the edges of the gridded data regions to ensure a smooth

interpolated transition between areas with different data sources. This TIN was linearly interpolated using ArcGIS 3D Analyst to produce intermediate 1 arc-second and 6 arc-second raster grid. The gridded datasets were then bilinearly resampled to these resolutions and overlaid on top of the intermediate grids.

3.3.2 Keauhou DEM in 1/3-arc-sec resolution

A high-resolution DEM in 1/3-arc-sec (~10m) was developed for the Keauhou area by the National Geophysical Data Center (Carignan et al., 2011). The DEM was generated from diverse digital datasets in the region (grid boundary and sources shown in Fig. 7b). The topographical Lidar data from State of Hawaii Civil Defencse /FEMA and HI DBEDT have approximately 1 m special resolution. The detail of the data sources and methodology used in developing the Keauhou DEM can be found in (Carignan et al., 2011).

3.4 Model Setup

By sub-sampling from the DEMs described in section 3.3, two sets of computational grids were derived for Keauhou, a reference inundation model (Fig. 8) and the optimized forecast model (Fig.9). The reference grids consist of three levels of telescoped grids with increasing resolution. The regional grid covers the major Hawaiian Islands (Fig. 8a), and the coastal grids the Island of Hawaii (Fig. 8b). Run-up and inundation simulations are computed on the coastline (Fig. 8c). The optimized forecast model has three levels of telescoped grids(Fig. 9). Grid details at each level and input parameters are summarized in Table 3.

4 Results and discussion

4.1 Validation, Verification, and Testing of the Forecast Model

Since no tide gage data was available at Keauhou, we evaluate the forecast model performance through comparison of tsunami amplitude time series, maximum amplitude and current at the forecast area to the results from the reference model

Both the reference and the forecast models for Keauhou were tested with the seventeen past tsunamis summarized in Table 2. Figures 10 shows the comparisons of modeled amplitude time series at the warning point computed by the reference and forecast models. The computed maximum water elevation above MHW and maximum current of the seventeen tsunamis are plotted in Figure 11. The 2011 Japan tsunami generated the largest amplitude at the warning point (1 m) as well as in the forecast area.

Recorded historical tsunamis provide only a limited number of events, from limited locations. More comprehensive test cases of destructive tsunamis with different

directionalities are needed to check the stability and robustness for the forecast model. The same set of eighteen simulated magnitude 9.3 tsunamis as in Tang *et al*. (2008[a], 2009[b]) was selected here for further examination (Table 4). Results computed by the forecast model are compared with those from the high-resolution reference model in Table 4, Figures 12 and 13. Both models were numerically stable for all of the scenarios. Waveforms computed by the forecast model agree well with those from the reference model (Fig. 12). Both models compute similar maximum water elevation and inundation in the study area (Fig. 13). These results indicate the forecast model is capable of providing robust and stable predictions of long duration for Pacific-wide tsunamis.

The No. 1 Japan, No. 2 Kamchatka, No. 10 Southern Chile, and No. 12 Northermn Tonga scenario from produced inundation at Keauhou. The computed maximum wave amplitude reaches 3.6 m at the warning point of the Japan scenario. Tsunami waves in the study area vary significantly for the eighteen magnitude 9.3 scenarios. These results show the complexity and high nonlinearity of tsunami waves nearshore, which again demonstrate the value of the forecast model for providing accurate site-specific forecast details.

4.2 Uncertainty of the forecast results

Figure 14 shows the difference of the maximum wave amplitude at the warning point between the forecast and reference models for the 35 scenarios, which includes the 17 past tsunamis and 18 simulated M_w 9.3 scenarios. In general, the forecast model shows smaller maximum amplitudes than those from the reference model. The difference of the maximum amplitude at the warning point between the reference and forecast models is within 17 cm when it is under 1 m (except the 1946 tsunami, which shows a 31 cm difference for a maximum amplitude of 65 cm), and less than 20% when it is greater than 1 m (except the magnitude 9.3 tsunamis from Central Aleutian, Kamchatka and Izu subdection zones, from which the difference can be 33%).

5 Summary and Conclusions

A tsunami forecast model was developed for the coastal community of Keauhou, Hawaii. The computational grids for the Keauhou forecast model were derived from the best available bathymetric and topographic data sources. The forecast model is optimizedly constructed at a resolution of 1-arc-sec (~30 m) to enable a 4-hr inundation simulation in minutes of computational time. A reference inundation model of higher resolution of 1/3 arc-sec (~10 m) was also developed in parallel, to provide modeling references for the forecast model. Both models were tested for seventeen past tsunamis and a set of eighteen simulated magnitude 9.3 tsunamis.

The optimized forecast model can provide a 4-hour site-specified forecast of first wave arrival, amplitudes and reasonable inundation limit in minutes of receiving tsunami source information constrained by deep-ocean DART measurements.

A tsunami could strike Keauhou with large waves from the Japan, Kamchatka and Northern Tonga, and Southern Chile subduction zones. Attention also needs to be paid to locations from which the main offshore wave energy propagates towards Hawaiian Islands, including the Alaska-Aleutian, Canada, Cascadia, South America and Vanuatu subduction zones. The water front at Kahaluu Beach Park and area at end of Keauhou bay are under high flooding risk once inundation occurs in the forecast area.

Acknowledgements

The author thanks Elena Tolkova, Jean Newman for assistance; and Sandra Bigley for comments, discussion and editing; Burak Uslu for providing tables and graphics for the propagation database. Collaborative contributions of the National Weather Service, the National Geophysical Data Center, and the National Data Buoy Center were invaluable.

Funding for this publication and all work leading to development of a tsunami forecast model for Keauhou, Hawaii was provided by the National Oceanic and Atmospheric Administration. This publication was partially funded by the Joint Institute for the Study of the Atmosphere and Ocean (JISAO) under NOAA Cooperative Agreement No. NA17RJ1232, JISAO Contribution No. xxxx. This is PMEL Contribution No. xxxx.

References

Bernard, E.N., H.O. Mofjeld, V.V. Titov, C.E. Synolakis, and F.I. González (2006): Tsunami: Scientific frontiers, mitigation, forecasting, and policy implications. Proc. Roy. Soc. Lon. A, 364(1845), doi: 10.1098/rsta.2006.1809, 1989–2007.

Bernard, E., and V.V. Titov (2007), Improving tsunami forecast skill using deep ocean observations, Mar. Technol. Soc. J., 40(3), 23–26.

Bracken, S. (2011): Tsunami Cleanup Update. Big Island News Center, March 19, 2011, http://www.bigislandnewscenter.com/tsunami-cleanup-update/.

Carignan, K.S., L.A. Taylor, B.W. Eakins, D.Z. Friday, P.R. Grothe, E. Lim and M. Love (2011): Digital Elevation Models of Keauhou and Kawaihae, Hawaii: Procedures, Data Sources and Analysis. NOAA National Geophysical Data Center (NGDC).

Gica E., Spillane, M.C., Titov, V.V., Chamberlin, C.D. and Newman, J.C. (2008), Development of the forecast propagation database for NOAA's Short-Term Inundation Forecast for Tsunamis (SIFT), NOAA Tech. Memo. OAR PMEL-139, 89pp.

Gusiakov, V.K. (1978): Static displacement on the surface of an elastic space. Ill-posed problems of mathematical physics and interpretation of geophysical data, Novosibirsk, VC SOAN SSSR, 23–51 (in Russian).

Gonzalez, F.I., E.N. Bernard, C. Meinig, M. Eble, H.O. Mofjeld, and S. Stalin (2005): The NTHMP tsunameter network. *Nat. Hazards*, 35(1), Special Issue, U.S. National Tsunami Hazard Mitigation Program, 25-39.

Kanamori, H. and J.J. Ciper (1974): Focal process of the great Chilean earthquake, May 22, 1960. *Physics of the Earth and Planetary Interiors*, 9, 128-136.

Lander, J. F. and P.A. Lockridge (1989): *United States Tsunamis 1690-1988*. NOAA National Environmental Satellite, Data and Information Service, National Geophysical Data Center, Boulder, Colorado, August 1989, 265pp.

Liu, P. L.-F. (2009), Tsunami modeling—Propagation, in The Sea, vol. 15, edited by E. Bernard and A. Robinson, chap. 9, pp. 295– 319, Harvard Univ. Press, Cambridge, Mass.

López, A.M. and E.A. Okal (2006), A seismological reassessment of the source of the 1946 Aleutian 'tsunami' earthquake, *Geophysical Journal International*, Volume 165, Issue 3, Page 835-849, Jun 2006, doi: 10.1111/j.1365-246X.2006.02899.x

National Geophysical Data Center, Global Tsunami Database (2000 BC to present):

http://www.ngdc.noaa.gov/seg/hazard/tsu_db.shtml

Okada, Y., 1985, Surface deformation due to shear and tensile faults in a half-space. *Bull. Seismol. Soc. Am*., 75, 1135-1154.

Rizzuto, J. (2011): Tsunami Hits Keauhou Bay Hard, Big Island News Center, March 13, 2011, http://www.bigislandnewscenter.com/tsunami-hits-keauhou-bay-hard/.

Satake, K., Y. Hasegawa, Y. Nishimae and Y. Igarashi (2008), Recent Tsunamis That Affected the Japanese Coasts and Evaluation of JMA's Tsunami Warnings. OS42B-03, AGU Fall Meeting, San Francisco.

Smith, W. H. F., and D. T. Sandwell (1997), Global seafloor topography from satellite altimetry and ship depth soundings, Science, 277, 1957– 1962.

Soloviev, S.L. and Ch.N Go (1984): *Catalog of Tsunamis on the Eastern Shore of Pacific Ocean*. Canadian Translation of Fisheries and Aquatic Sciences, No. 5078, 293 pp.

Soloviev, S.L., Ch.N Go and Kh.S Kim (1992): *Catalog of Tsunamis in The Pacific* 1969-1982. Results of Researches on The International Geophysical Projects, Academy of Sciences of the USSR Soviet Geophysical Committee, Moscow, 1992, 208 pp.

Synolakis, C.E., E.N. Bernard, V.V. Titov, U. Kânoğlu, and F.I. González (2008): Validation and verification of tsunami numerical models. *Pure Appl. Geophys*., 165(11–12), 2197–2228.

Tang, L., C. Chamberlin, E. Tolkova, M. Spillane, V.V. Titov, E.N. Bernard, and H.O. Mofjeld (2006): Assessment of potential tsunami impact for Pearl Harbor, Hawaii. NOAA Tech. Memo. OAR PMEL-131.

Tang, L., C. Chamberlin and V.V. Titov, (2008a), Developing tsunami forecast inundation models for Hawaii: procedures and testing, *NOAA Tech. Memo., OAR PMEL -141*, 46 pp.

Tang, L., V.V. Titov, Y. Wei, H.O. Mofjeld, M. Spillane, D. Arcas, E.N. Bernard, C. Chamberlin, E. Gica, and J. Newman (2008b): Tsunami forecast analysis for the May 2006 Tonga tsunami. J. Geophys. Res., 113, C12015, doi: 10.1029/2008JC004922.

Tang, L., V. V. Titov, and C. D. Chamberlin (2009a), Development, Testing, and Applications of Site-specific Tsunami Inundation Models for Real-time Forecasting, *J. Geophys. Res*., doi:10.1029/2009JC005476, in press.

Tang, L., V.V. Titov and C.D. Chamberlin (2009b), A Tsunami Forecast Model for Hilo, Hawaii, NOAA OAR Special Report, PMEL Tsunami Forecast Series: Vol. 1, 44 pp.

Taylor, L.A., B.W. Eakins, K.S. Carignan, R.R. Warnken, T. Sazonova, and D.C. Schoolcraft, (2007): Digital Elevation Model for Keauhou, Hawaii: Procedures, Data Sources and Analysis, NOAA, National Geophysical Data Center, Boulder, Colorado, March 20, 2007, 21 pp.

Titov, V.V. (2009), Tsunami forecasting. Chapter 12 in *The Sea*, Volume 15: Tsunamis, Harvard University Press, Cambridge, MA and London, England, 371–400.

Titov, V.V., F.I. González, E.N. Bernard, M.C. Eble, H.O. Mofjeld, J.C. Newman, and A.J. Venturato (2005): Real-time tsunami forecasting: Challenges and solutions. *Natural Hazards*, 35(1), Special Issue, U.S. National Tsunami Hazard Mitigation Program, 41–58.

Titov, V. V., Mofjeld, H. O., Gonza´ lez, F. I., and Newman, J. C.: 2001, Offshore forecasting of Alaskan tsunamis in Hawaii. In: G. T. Hebenstreit (ed.), Tsunami Research at the End of a Critical Decade. Birmingham, England, Kluwer Acad. Pub., Netherlands, pp. 75–90.

Titov, V.V., H.O. Mofjeld, F.I. Gonzalez and J.C. Newman (1999): Offshore forecasting of Alaska-Aleutian subduction zone tsunamis in Hawaii. NOAA Technical Memorandum. ERL PMEL-114, January 1999, 22 pp.

Titov, V.V. and C.S. Synolakis (1998): Numerical modeling of tidal wave runup. *Journal of Waterway, Port, Coastal and Ocean Engineering*, ASCE, 124(4), 157-171.

Titov, V.V. and F.I. Gonzalez (1997): Implementation and testing of the Method of Splitting Tsunami (MOST) model. NOAA Technical Memorandum. NOAA Pacific Marine Environmental Laboratory, ERL PMEL-112, Nov. 1997, 11 pp.

Pararas-Carayannis, G.(1969): *Catalog of Tsunamis in The Hawaii Islands*, World Data Center A Tsunami, ESSA – Coast and Geodetic Survey, 94 pp.

Walker, D.A. (2004): Regional Tsunami evacuations for the state of Hawaii: a feasibility study on historical runup data. Science of Tsunami Hazards, 22(1), 3-22.

Wei, Y., E. Bernard, L. Tang, R. Weiss, V. Titov, C. Moore, M. Spillane, M. Hopkins, and U. Kânoğlu (2008): Real-time experimental forecast of the Peruvian tsunami of August 2007 for U.S. coastlines. *Geophys. Res. Lett*., 35, L04609, doi: 10.1029/2007GL032250.

Whitmore, P.M. (2003), Tsunami amplitude prediction during events: A test based on previous tsunamis. In *Science of Tsunami Hazards*, 21, 135–143.

Table 1 Tsunami source functions in the Pacific, Atlantic and Indian Oceans.

Source Zone			Tsunami source functions	
No.	**Abbr.**	**Name**	**Line/zone**	**Numbers**
1	ACSZ	Aleutian-Alaska-Canada-Cascadia	BAZYXW	184
2	CSSZ	Central-South American	BAZYX	382
3	EPSZ	East Philippines	BA	44
4	KISZ	Kamchatka-Kuril-Japan Trench-Izu Bonin-Marianas-Yap	BAZYXW	222
5	MOSZ	Manus Ocean Convergence Boundary	BA	34
6	NVSZ	New Britain-Solomons-Vanuatu	BA	74
7	NGSZ	North New Guinea	BA	30
8	NTSZ	New Zealand-Kermadec-Tonga	BA	78
9	NZSZ	South New Zealand	BA	14
10	RNSZ	New Ryukus-Kyushu-Nankai	BA	44
			Subtotal:	**1106**
11	ATSZ	Atlantic	BA	214
12	SSSZ	South Sandwich	BA	22
			Subtotal:	**236**
13	IOSZ	Adaman-Nicobar-Sumatra-Java	BAZY	307
14	MKSZ	Makran	BA	20
15	WPSZ	West Philippines	BA	22
			Subtotal:	**349**
			Total:	**1691**

Table 2 Tsunami sources for 16 past tsunamis. (**Please use the same Table 1 in the Kahului report, except reverse the order**)

No.	Tsunami ID	Area	Earthquake Date Time (UTC)	Location Lat (°)	Location Lon (°)	Source zone	Seismic moment magnitude (M_W)	Tsunami moment magnitude (T_{Mw})	Tsunami source
1	194604	Unimak	1946.04.01 12:28:56	53.32N	163.19W	ACSZ	8.5 (Lopez & Okal, 2006)	[2]8.5	7.5*b23+19.7*b24+3.7*b25
2	195211	Kamchatka	1952.11.04 16:58:26.0	52.75N	159.50E	KISZ	9.0 (NGDC)	[2]8.7	
3	195703	Andreanof	1957.03.09 14:22:31	51.292N	175.629W	ACSZ	8.6 (NGDC)	[2]8.7	31.4*a15+10.6*a16+12.2*a17
4	196005	Chile	1960.05.22 19:11:14	39.5S	74.5W	SASZ	9.5 (Kanamori & Cipar ,1974)		
5	196403	Alaska	1964.03.28 03:36:14	61.10N	147.50W	ACSZ	9.2 (NGDC)	[2]9.0	Tang *et al*. (2006)
6	199410	West Kuril Is.	1994.10.04 13:23:28.5	43.60N	147.63E	KISZ	8.3 (CMT)	8.1	9.00*a20
7	199606	Andreanof	1996.06.10 04:04:3.4	51.1N	177.41W	ACSZ	7.9 (CMT)	7.8	2.40*a15+0.80*b16
8	200106	Peru	2001.06.23 20:34:23.3	17.28S	72.71W	SASZ	8.4 (CMT)	[2]8.2	5.70*a15+2.90*b16+1.98*a16
9	200309	Hokkaido	2003.09.25 19:50:38.2	42.21N	143.84E	KISZ	8.3 (CMT)	[2]8.0	3.6m*(100x100km), 109#rake, 20#dip, 230#strike, 25m depth
10	200311	Rat Is.	2003.11.17 06:43:31	51.14N	177.86E	ACSZ	7.7 (CMT)	[1]7.8	2.81*b11
11	200605	Tonga	2006.05.03 15:26:39	20.39S	173.47W	NTSZ	8.0 (CMT)	8.0	6.6*b29 (Tang *et al*., 2008[b])
12	200611	Central Kuril Is.	2006.11.15 11:15:8.0	46.71N	154.33E	KISZ	8.3 (CMT)	[1]8.1	4*a12+0.5*b12+2*a13+1.5*b13
13	200701	Central Kuril Is.	2007.01.13 04:23:48.1	46.17N	154.80E	KISZ	8.1 (CMT)	[2]7.9	-3.64*b13
14	200708	Peru	2007.08.15 23:41:57.9	13.73S	77.04W	SASZ	8.0 (CMT)	[1]8.1	4.1*a9+4.32*b9 (Wei *et al*., 2008)
15									
16									

1: The tsunami source was obtained during real time and applied to forecast.
2: Preliminary result.
3. Trough reached gage limit.

Table 3 MOST setups of Keauhou reference and forecast models.

Grid	Region	Reference Model				Forecast model		
		Coverage Lon. (^{0}E) Lat. (^{0}N)	Cell Size (")	Time Step (sec)		Coverage Lon. (^{0}E) Lat. (^{0}N)	Cell Size (")	Time Step (sec)
A	Hawaii	199.0 - 205.98 18.0 – 23.0	36 (699 x 500)	3	A	199 - 205.9667 18.0317 - 22.9983	120 (210 x 150)	11.05
B	Big Island	202.8483-205.3983 18.6933 - 21.4283	6 (1531 x 1642)	0.45	B	203.8200 - 204.1983 19.3358 - 20.3091	6 (228 x 585)	0.85
C	Keauhou	203.9689 -204.070 19.4983 - 19.6642	1/3 (1729 x 487)	0.15	C	204.0166 - 204.0410 19.5497 - 19.6122	1 (89 x 226)	0.85
Minimum offshore depth (m)		1				1		
Water depth for dry land (m)		0.1				0.1		
Manning coefficient		0.025				0.03		
Computational time for a 4-hr simulation		~ 12 hours				**14 minutes**		

Table 4 Sources of the 18 Mw 9.3 synthetic tsunamis and model results at the Keauhou warning point computed by the reference and forecast models.

No.	Subd. Zone	Source	alpha	Ref. model η_{max} (m)	Ref. model t_{max} (hour)	Forecast Model η_{max} (m)	Forecast Model t_{max} (hour)	Location
1	KISZ	AB	22-31	3.57	7.999	3.03	8.004	Japan
2	KISZ	AB	1-10	2.66	8.049	1.78	8.036	Kamchatka
3	ACSZ	AB	16-25	1.71	5.349	1.22	4.882	Central Aleutian
4	ACSZ	AB	22-31	0.75	5.117	0.64	5.099	Unimak
5	ACSZ	AB	50-59	1.10	6.899	1.59	6.662	Canada
6	ACSZ	AB	56-65	0.87	7.416	0.92	6.681	Cascadia
7	CSSZ	AB	1-10	0.32	11.717	0.25	17.448	Central American
8	CSSZ	AB	41-50	0.29	12.299	0.29	12.289	Columbia-Ecuador
9	CSSZ	AB	86-95	0.77	16.133	0.72	16.085	Chile
10	CSSZ	AB	100-109	2.25	16.899	2.13	16.373	Southern Chile
11	NTSZ	AB	20-29	0.59	7.950	0.62	10.665	Tonga
12	NTSZ	AB	30-39	2.37	5.867	2.32	5.869	Northern Tonga
13	NVSZ	AB	28-37	1.04	8.033	1.01	8.033	Vanuatu
14	MOSZ	AB	1-10	1.11	8.300	1.07	8.327	Manus
15	NGSZ	AB	3-12	0.69	14.133	0.23	9.948	New Guinea
16	EPSZ	AB	6-15	1.90	11.767	1.52	11.774	East Philippines
17	RNSZ	AB	12-21	0.89	10.566	0.73	10.569	Nankai
18	KISZ	AB	32-41	2.34	9.200	1.65	8.288	Izu

Appendix A.

The following appendix lists the input files for Keauhou developed in 2011.

A1. Reference model *.in file for Keauhou , Hawaii for MOST version 4.0

A.
0.001 Minimum amplitude of input offshore wave (m):
1 Input minimum depth for offshore (m)
0.1 Input "dry land" depth for inundation (m)
0.0009 Input friction coefficient (n**2)
2 Number of grids
2 Interpolation domain for outer boundary
2 inner boundary
RA_hawaii_36s_20070806.nc
RB_kawaihae_B6s_20070806.nc
1
3 Input time step (sec)
9600 Input amount of steps
0 COntunue after input stops
20 Input number of steps between snapshots
1 saving inner boundaries every n-th timestep
1 ...Saving grid every n-th node, n=
./
/home/tg23/data/tang/store_c2/pacific_prop_db/2003_Hokkaido/sim_src/

B
0.002 Minimum amplitude of input offshore wave (m):
-300 Input minimum depth for offshore (m)
0.1 Input "dry land" depth for inundation (m)
0.0009 Input friction coefficient (n**2)
2 Number of grids
2 Interpolation domain for outer boundary
2 inner boundary
RB_kawaihae_B6s_20070806.nc
RC_keauhou_10m.nc
1
0.45 Input time step (sec)
64000 Input amount of steps
0 COntunue after input stops
133 Input number of steps between snapshots
1 saving inner boundaries every n-th timestep
1 ...Saving grid every n-th node, n=
./
./

C
0.002 Minimum amplitude of input offshore wave (m):
-300 Input minimum depth for offshore (m)
0.1 Input "dry land" depth for inundation (m)
0.0009 Input friction coefficient (n**2)
1 Number of grids
2 Interpolation domain for outer boundary
2 inner boundary

```
RC_keauhou_10m.nc
2
0.15      Input time step (sec)
192000    Input amount of steps
0             COntunue after input stops
400    Input number of steps between snapshots
1      saving inner boundaries every n-th timestep
1       ...Saving grid every n-th node, n=
./
./
```

A2. Forecast model *.in file for Keauhou, Hawaii for MOST version 2.0

```
0.0001    Minimum amplitude of input offshore wave (m):
1         Input minimum depth for offshore (m)
0.1       Input "dry land" depth for inundation (m)
0.000625  Input friction coefficient (n**2)
1         runup flag for grids A and B (1=yes,0=no)
300.0     blowup limit
0.85      Input time step (sec)
21176     Input amount of steps
13        Compute "A" arrays every n-th time step, n=
1         Compute "B" arrays every n-th time step, n=
26        Input number of steps between snapshots
1       ...Starting from
1       ...Saving grid every n-th node, n=
hawaii_2min_20070806.asc.s.c
FB_keauhou_6s2_20110602.most
FC_Keauhou_1s3_20110512.c
/home/tg23/data/tang/src_nc/src_sim_test/hawa/
./
1 1 1 1
1
1 76 183  keauhou 204.03740740  19.5616666 depth  m: 3.60
```

Figures

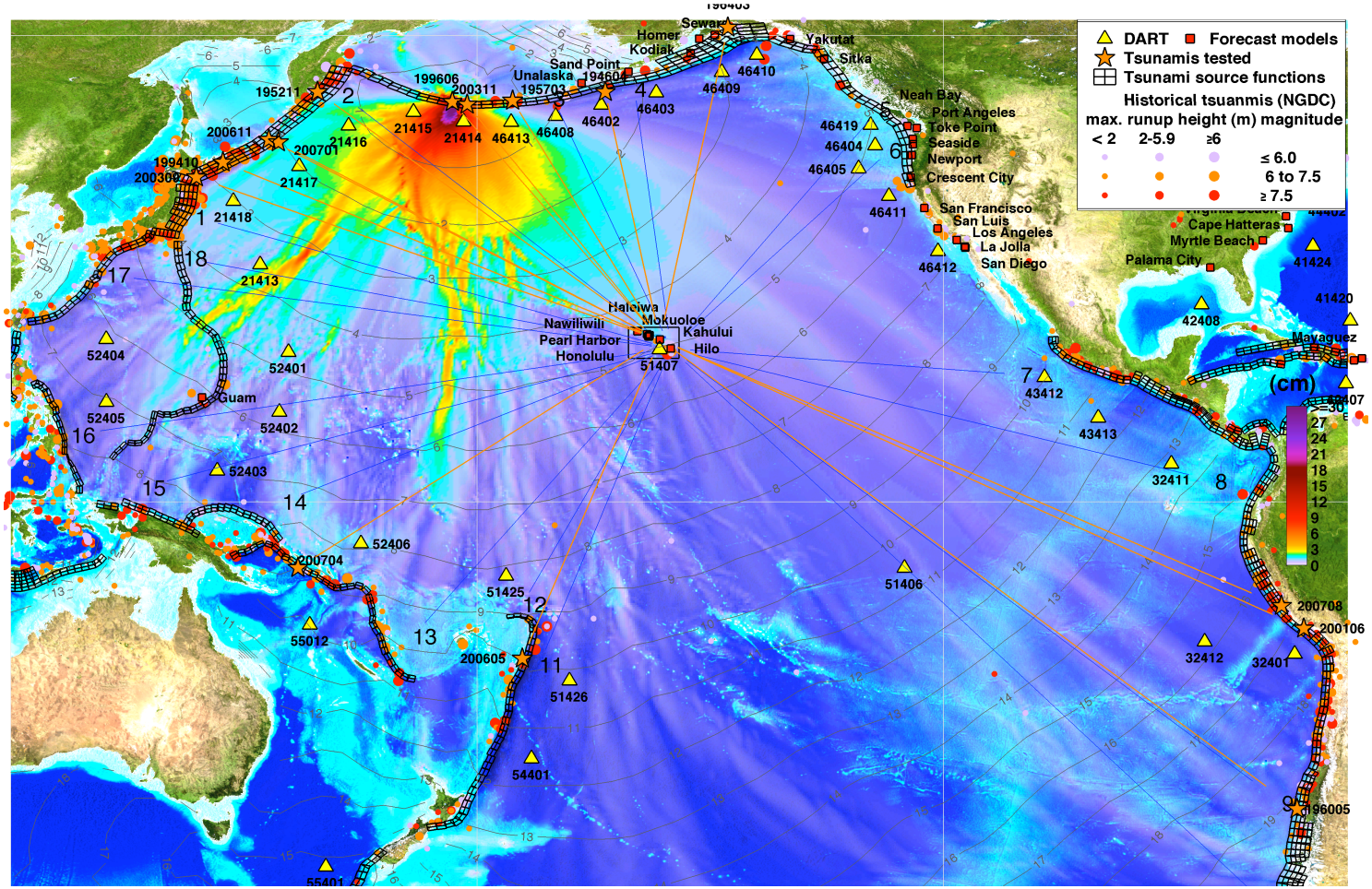

Figure 1 Overview of the Tsunami Forecast System in Pacific. System components include DART system (yellow triangles), pre-computed tsunami source function (unfilled black rectangles) and high-resolution forecast models (red squares). Colors show the offshore forecast of the computed maximum tsunami amplitude in cm for the 17 November 2003 Rat Islands tsunami in the Pacific. Contours indicate the travel time in hours. ——, seventeen past tsunamis and——, eighteen simulated magnitude 9.3 tsunamis tested in this study.

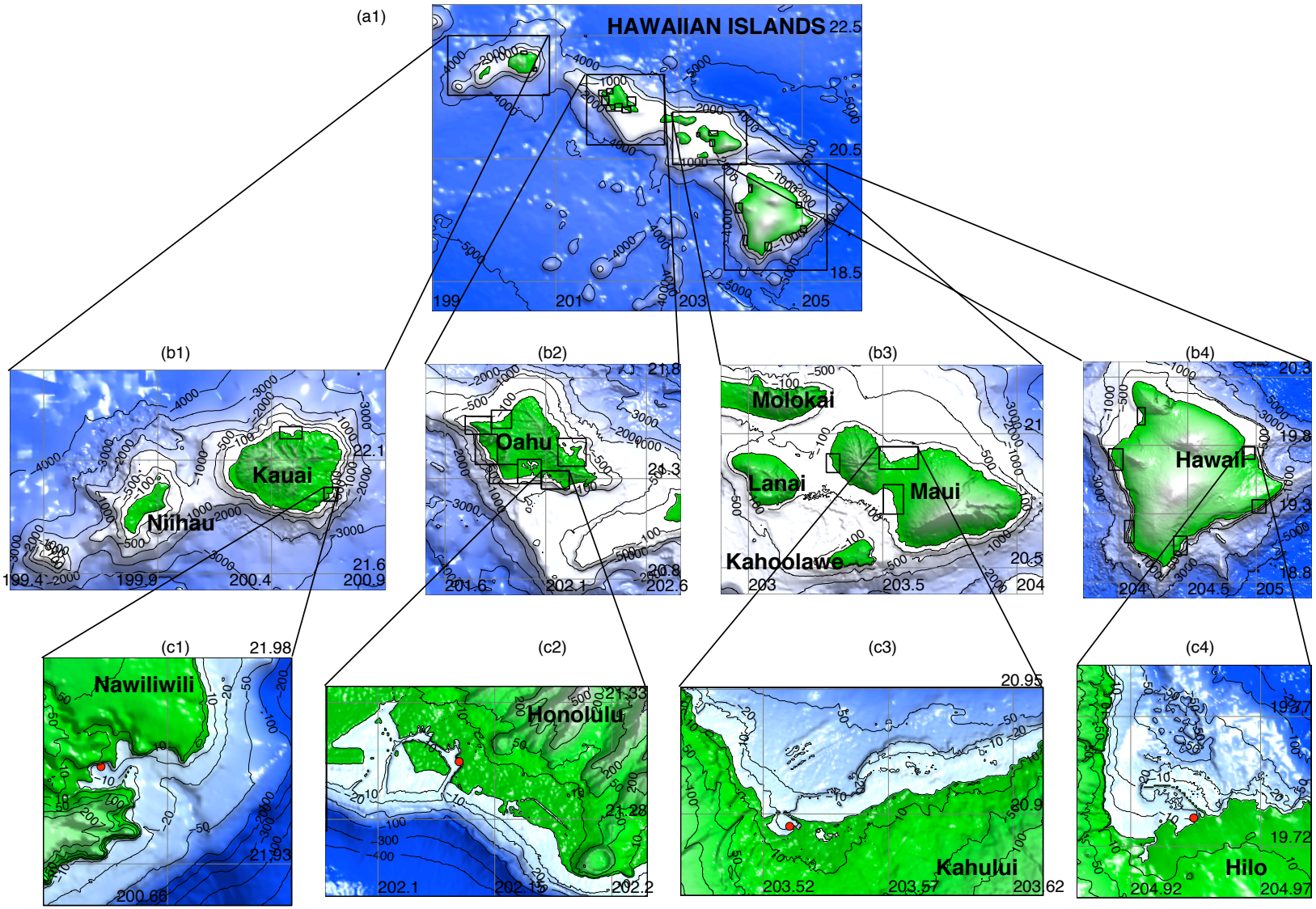

Figure 2 Forecast model setups for several forecast sites in Hawaii: (a) 2-arc-min (~3600m) regional, (b) 12-18-arc-sec (~360-540m) intermediate and (c) 2-arc-sec (~60m) nearshore grids for Nawiliwili, Honolulu, Kahului and Hilo. Red dots, coastal tide stations; red pluses, offshore locations.

Figure 3 An aerial photo of Keauhou (Image courtesy http://www.soest.hawaii.edu/coasts/).

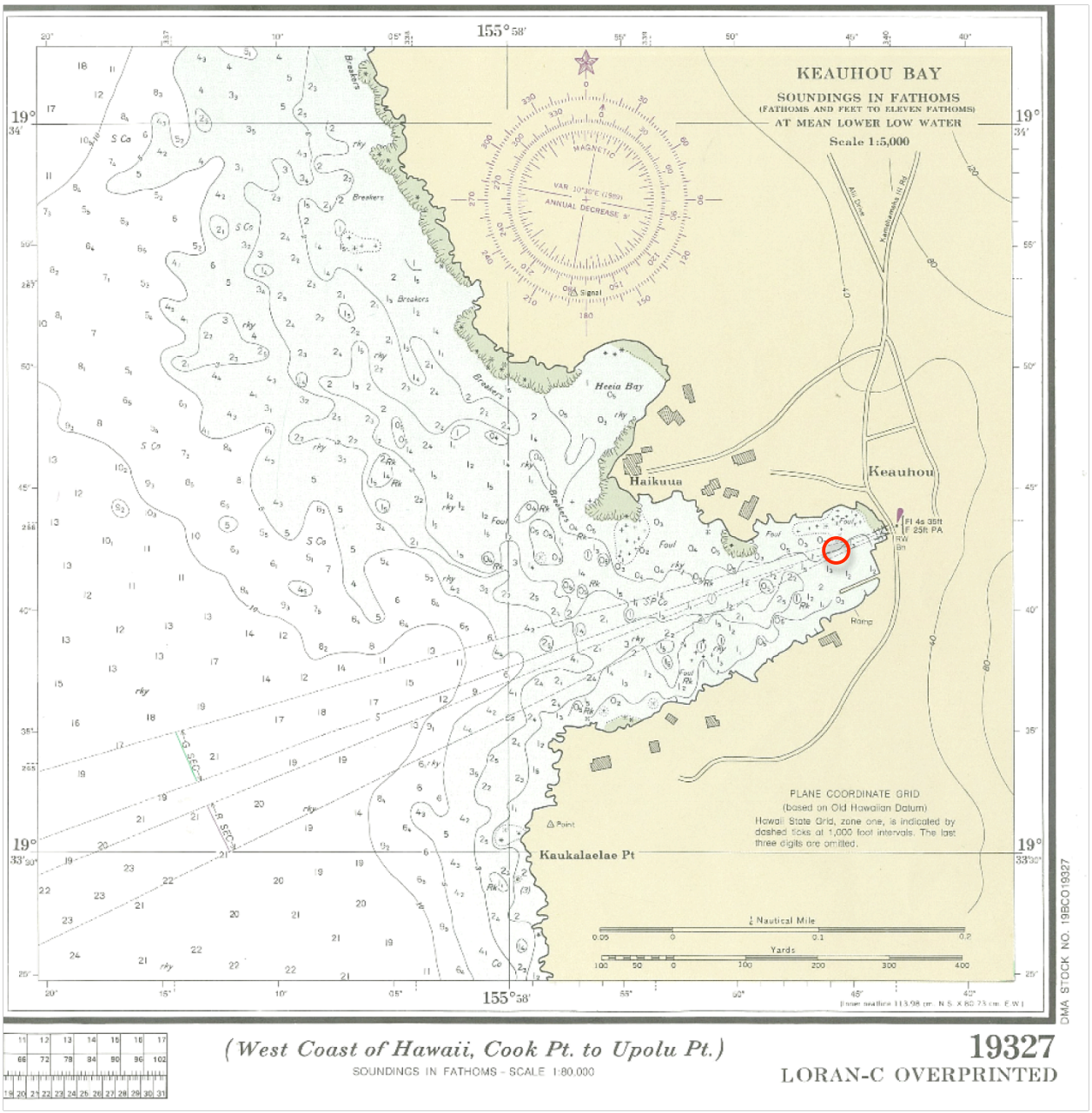

Figure 4 A chart of Keauhou (NOAA Chart 19327). Soundings in fathoms at Mean Lower Low Water. Contour and summit elevation values ate in feet above Mean Sea Level. Red Circle, Keauhou warning point.

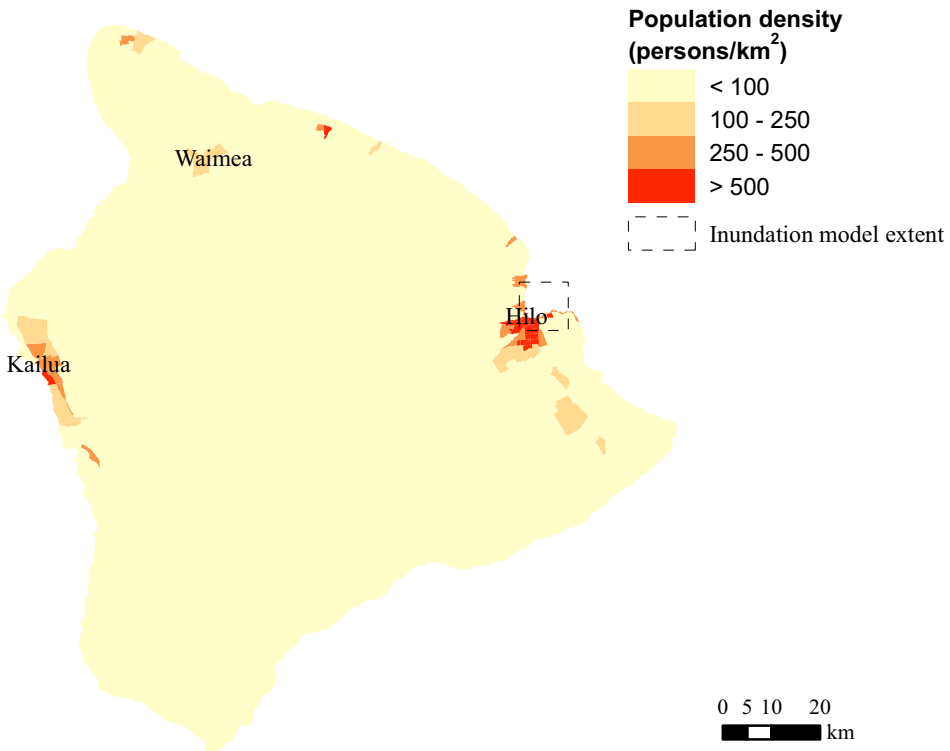

Figure 6 Population density, Hawaii. (Source: 2000Census)

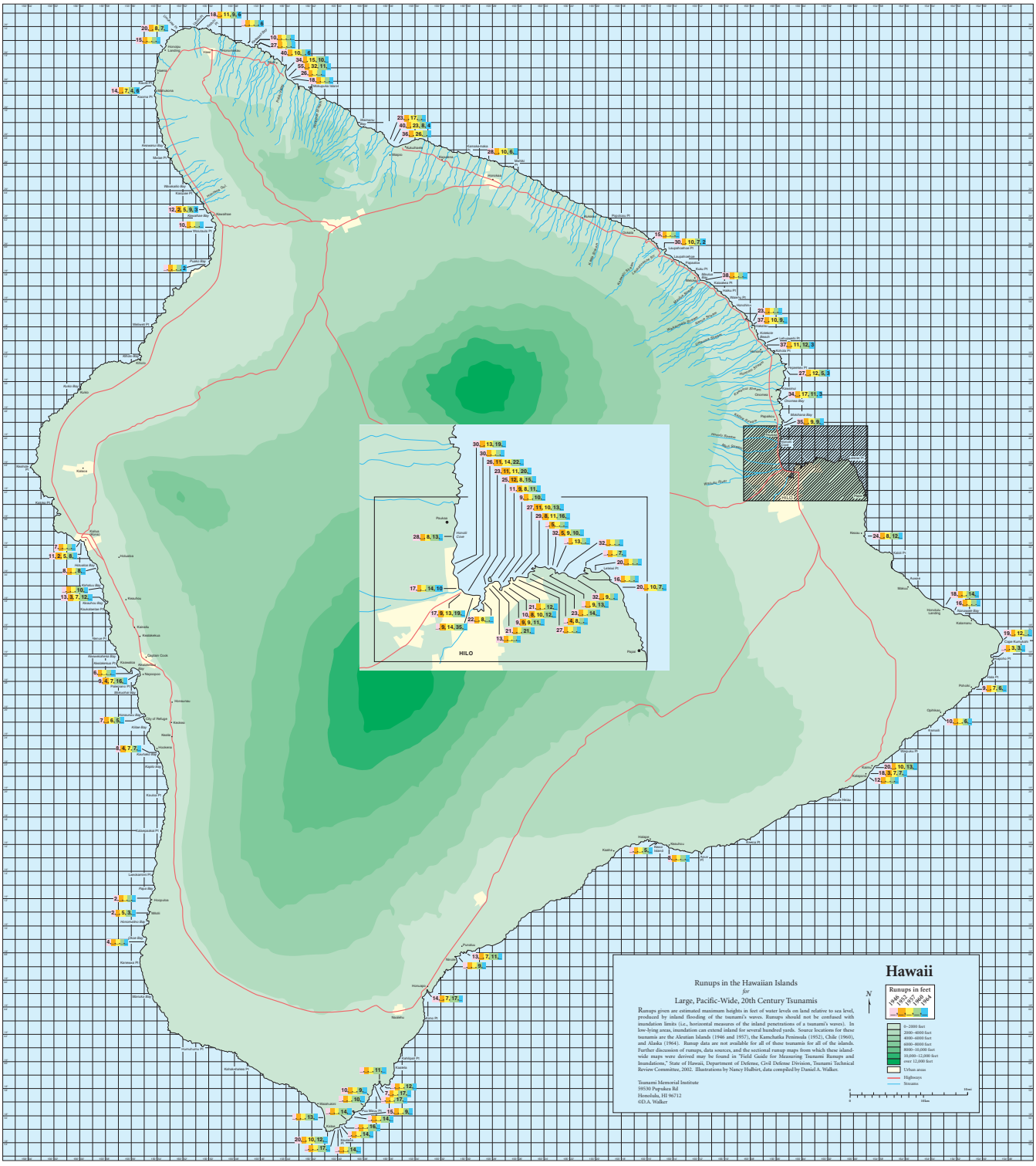

Figure 5 Run-ups in the Island of Hawaii for the 1946, 1957, 1960 and 1964 tsunamis (Image from Walker, 2004).

(a)

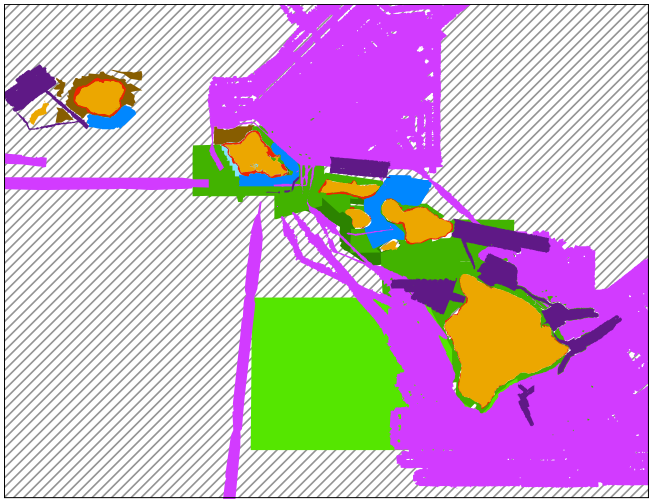

SHOALS LIDAR
JAMSTEC multibeam
MBARI multibeam
Navy multibeam
NOS digital echosounder
NOS multibeam
NOS lead-line surveys
USACE digital echosounder
USGS Seafloor Mapping Project multibeam
NOS nautical chart digitized contours
USGS GLORIA tracklines/Smith & Sandwell
NOAA CSC IfSAR topography
USGS National Elevation Dataset topography

(b)

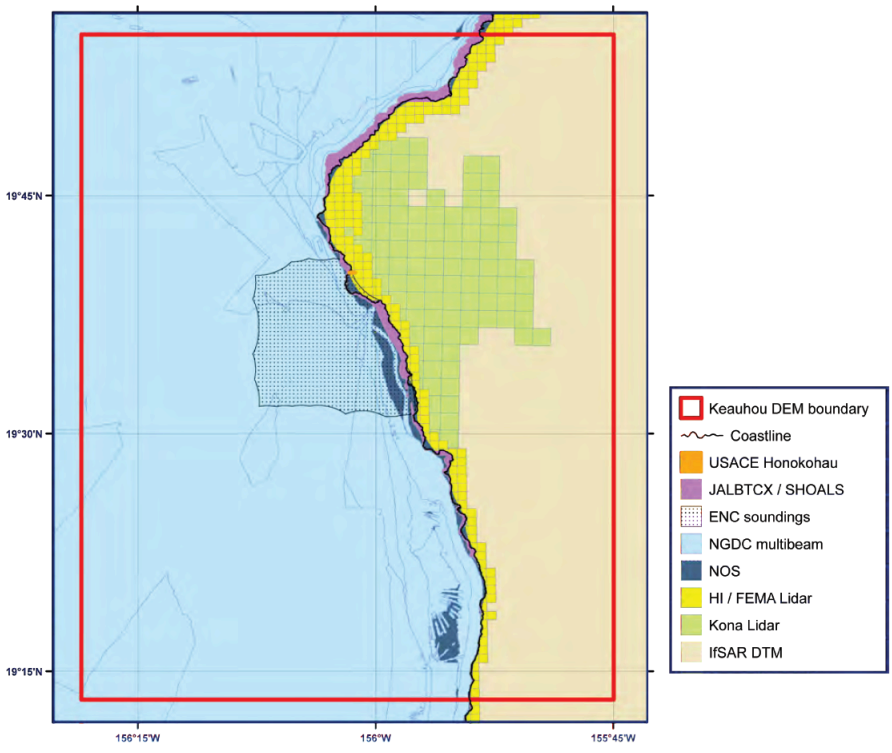

Figure 7 Bathymetric and topographic data source overview. (a) 6" sec (~180m) Hawaii DEM developed at NCTR; (b) 1/3" (~10m) Keauhou DEM developed by NGDC (Image courtesy Carignan et al., 2011).

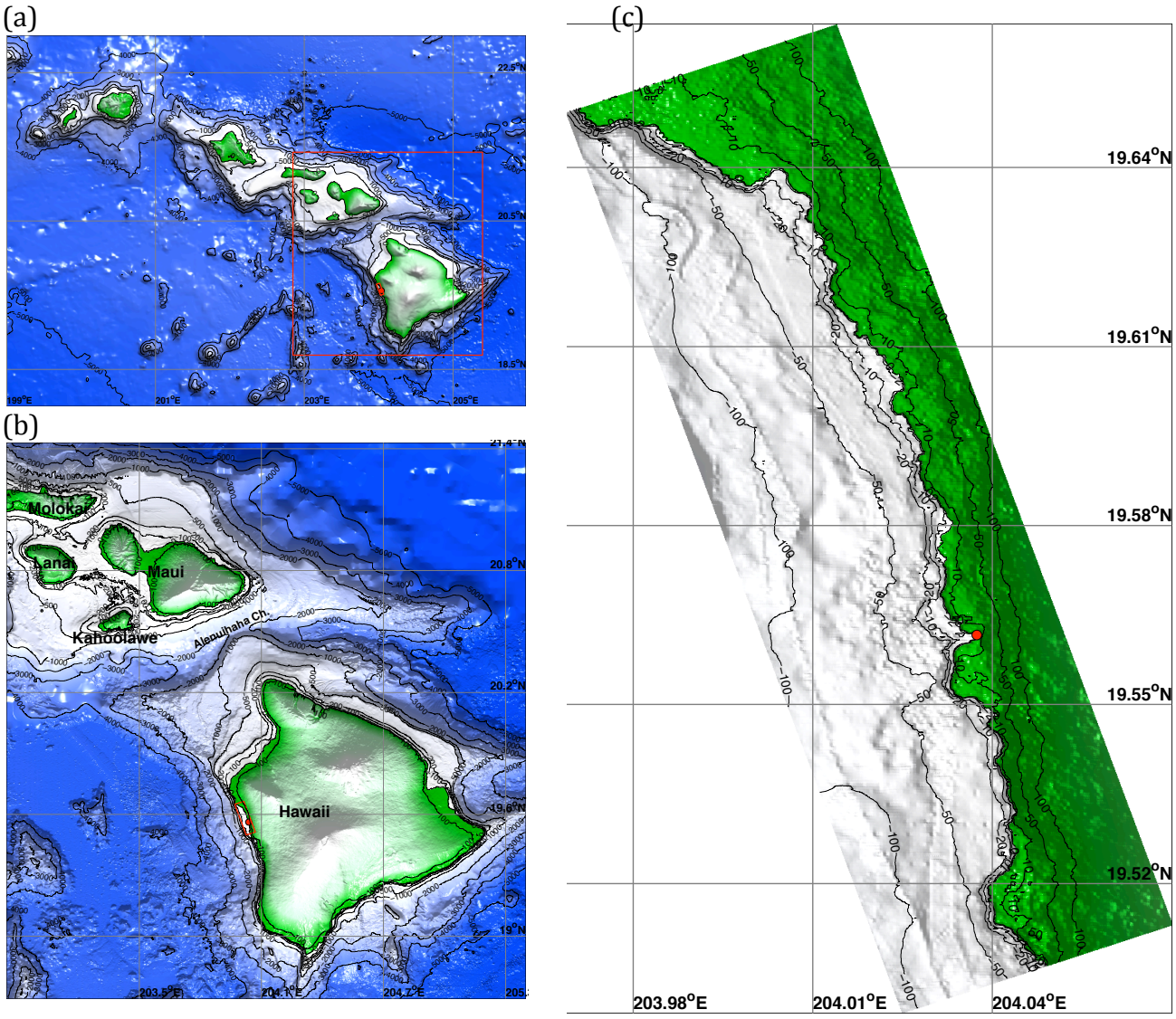

Figure 8 Grid setup of the Keauhou reference model with resolutions of (a) 36" (1080m), (b) 6" (180m),(c) 2" (60m) and (d) 1/3" (10m). □, nested grid boundary; ● Keauhou warning point .

(a)

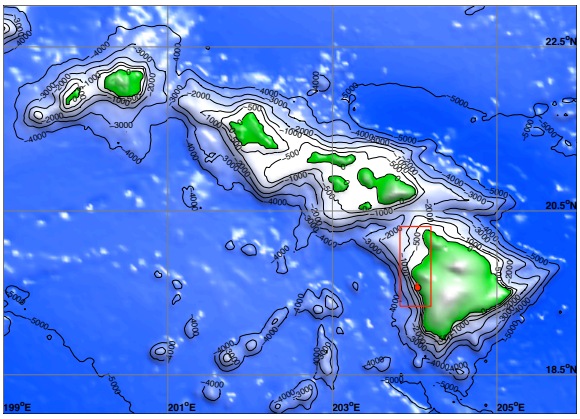

(b)

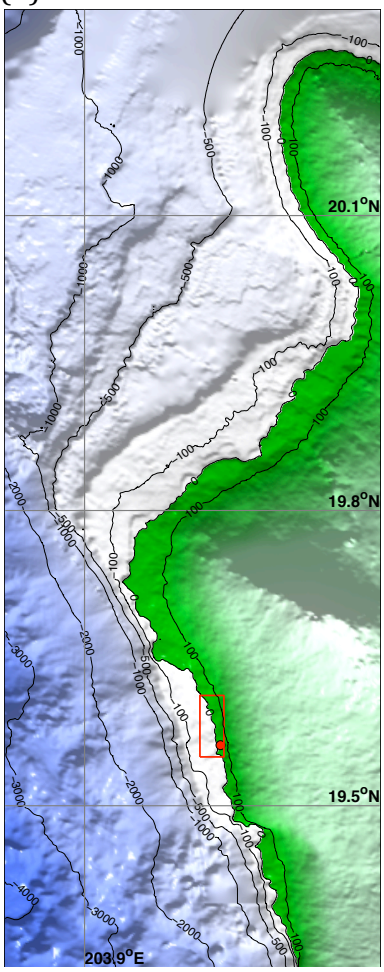

(c)

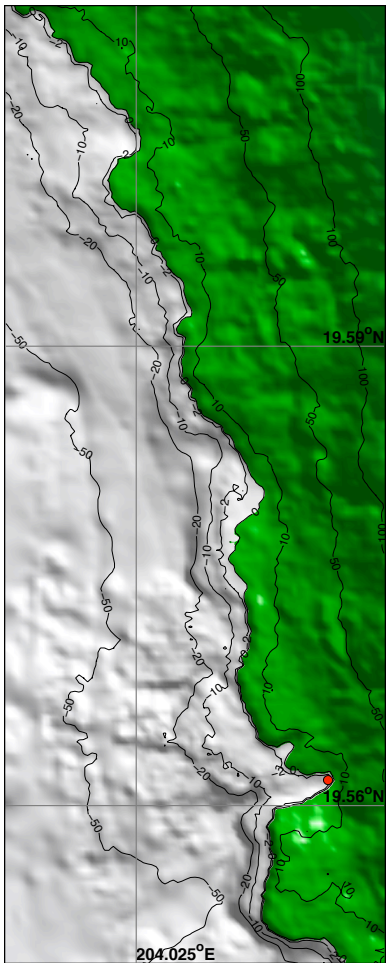

Figure 9 Grid setup of the Lahaina forecast model with resolutions of (a) 120" (3600m), (b) 6" (180m) and (c) 1" (30m). □, nested grid boundary; ●, Keauhou warning point at 204.03740740°E, 19.5616666°N, water depth of 3.5 m.

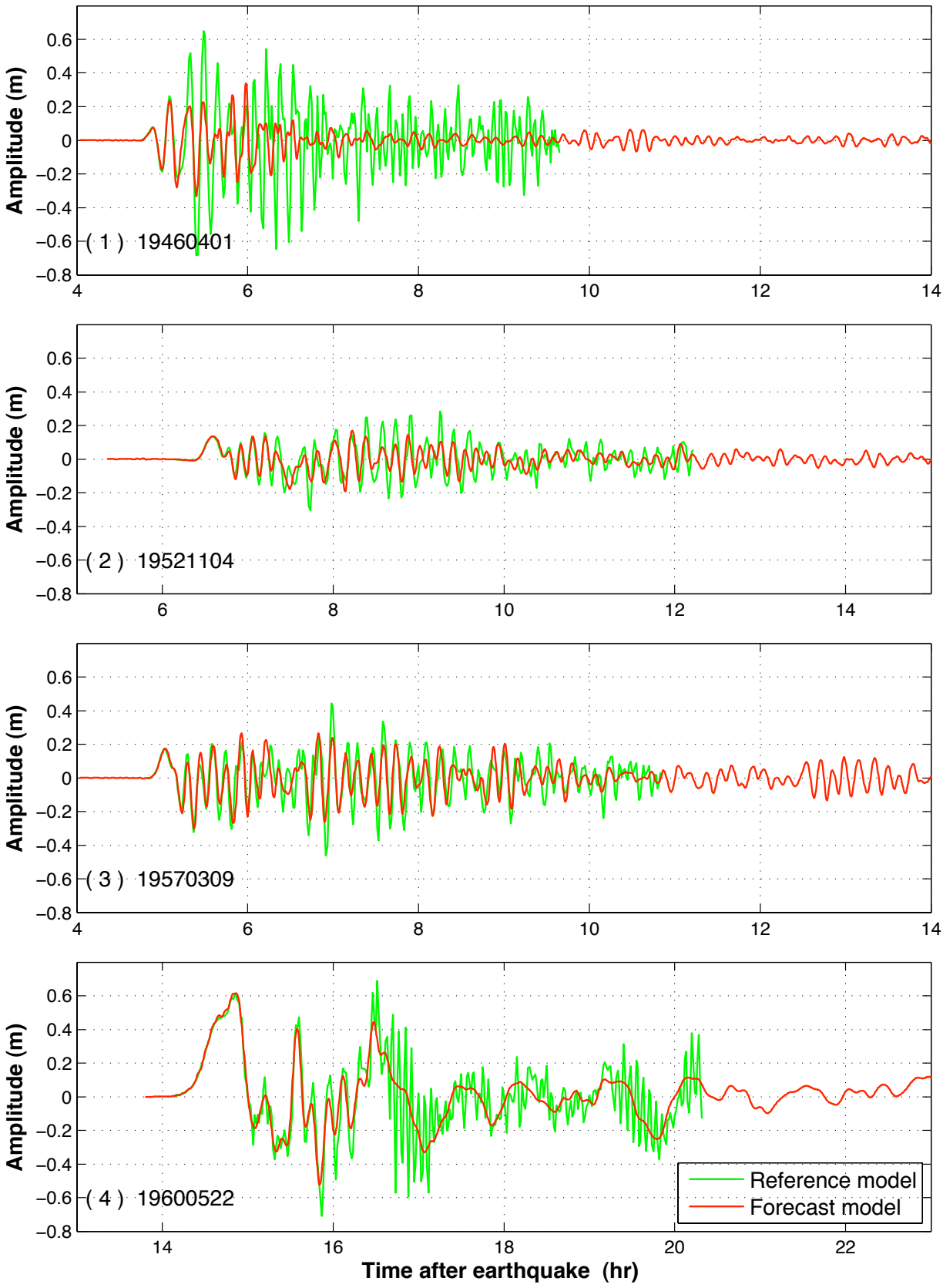
Amplitude (m)
(1) 19460401
(2) 19521104
(3) 19570309
(4) 19600522
Reference model
Forecast model
Time after earthquake (hr)

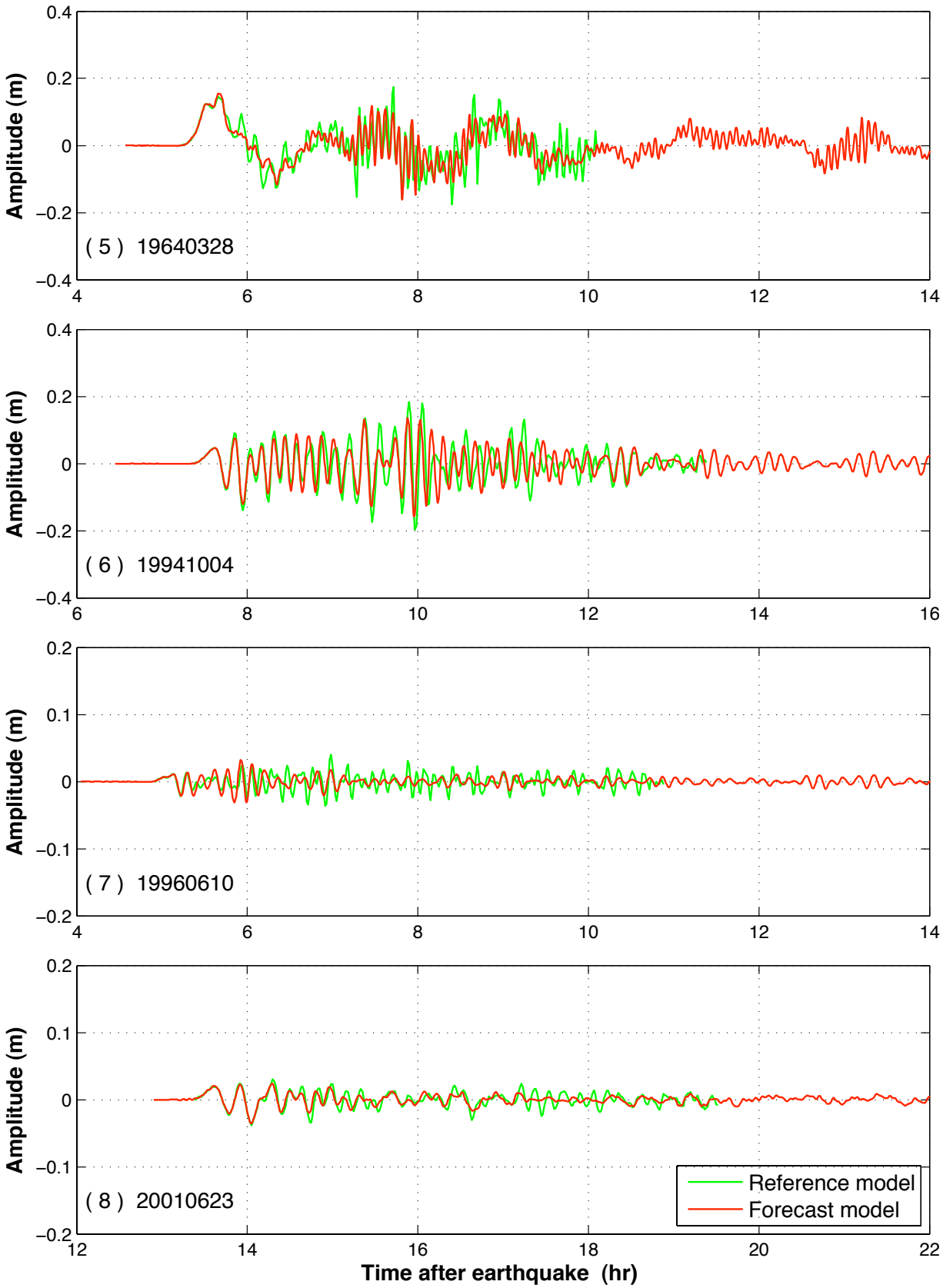
Amplitude (m)
(5) 19640328
(6) 19941004
(7) 19960610
(8) 20010623
Reference model
Forecast model
Time after earthquake (hr)

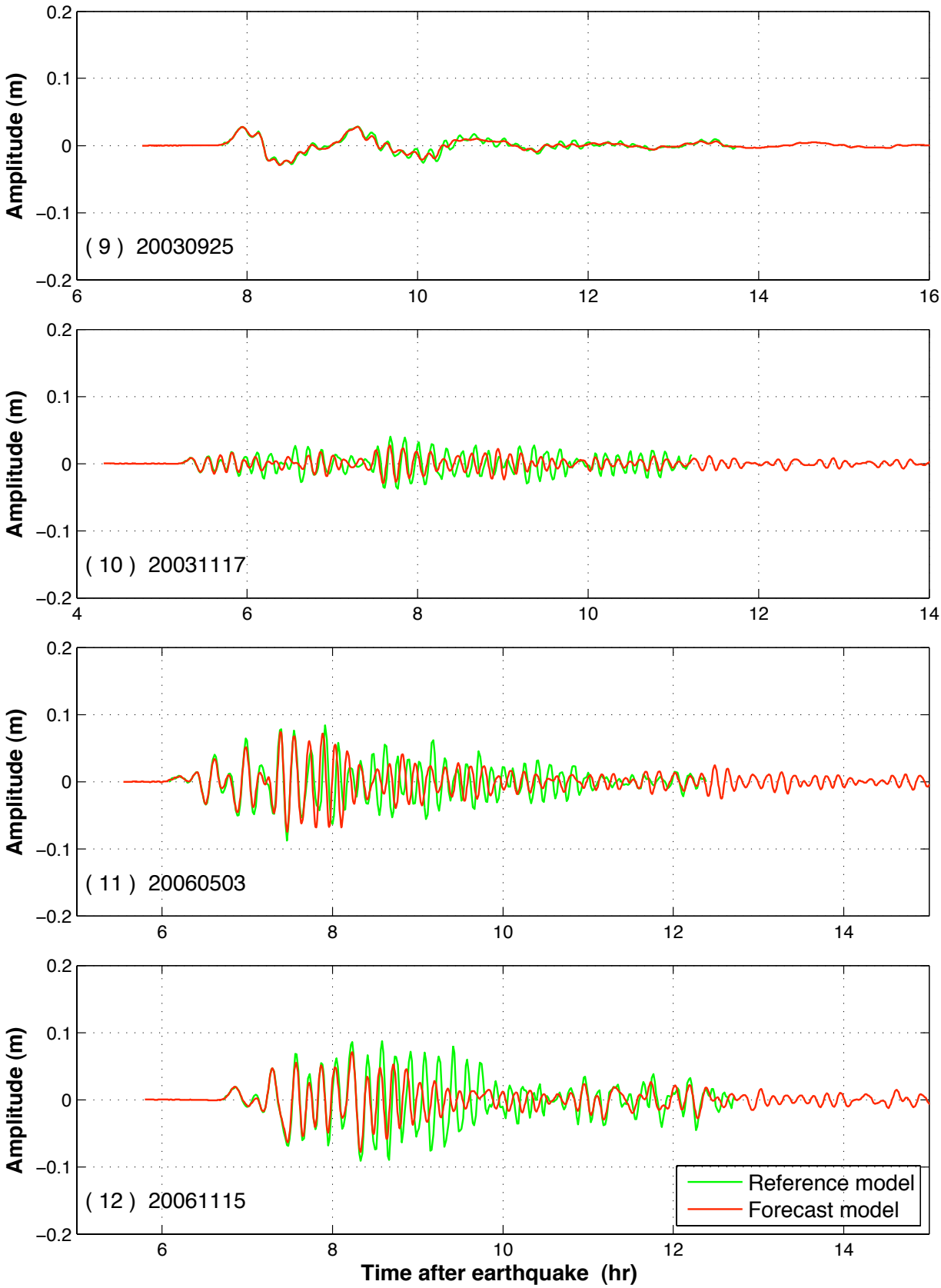
Amplitude (m)
(9) 20030925
(10) 20031117
(11) 20060503
(12) 20061115
Reference model
Forecast model
Time after earthquake (hr)

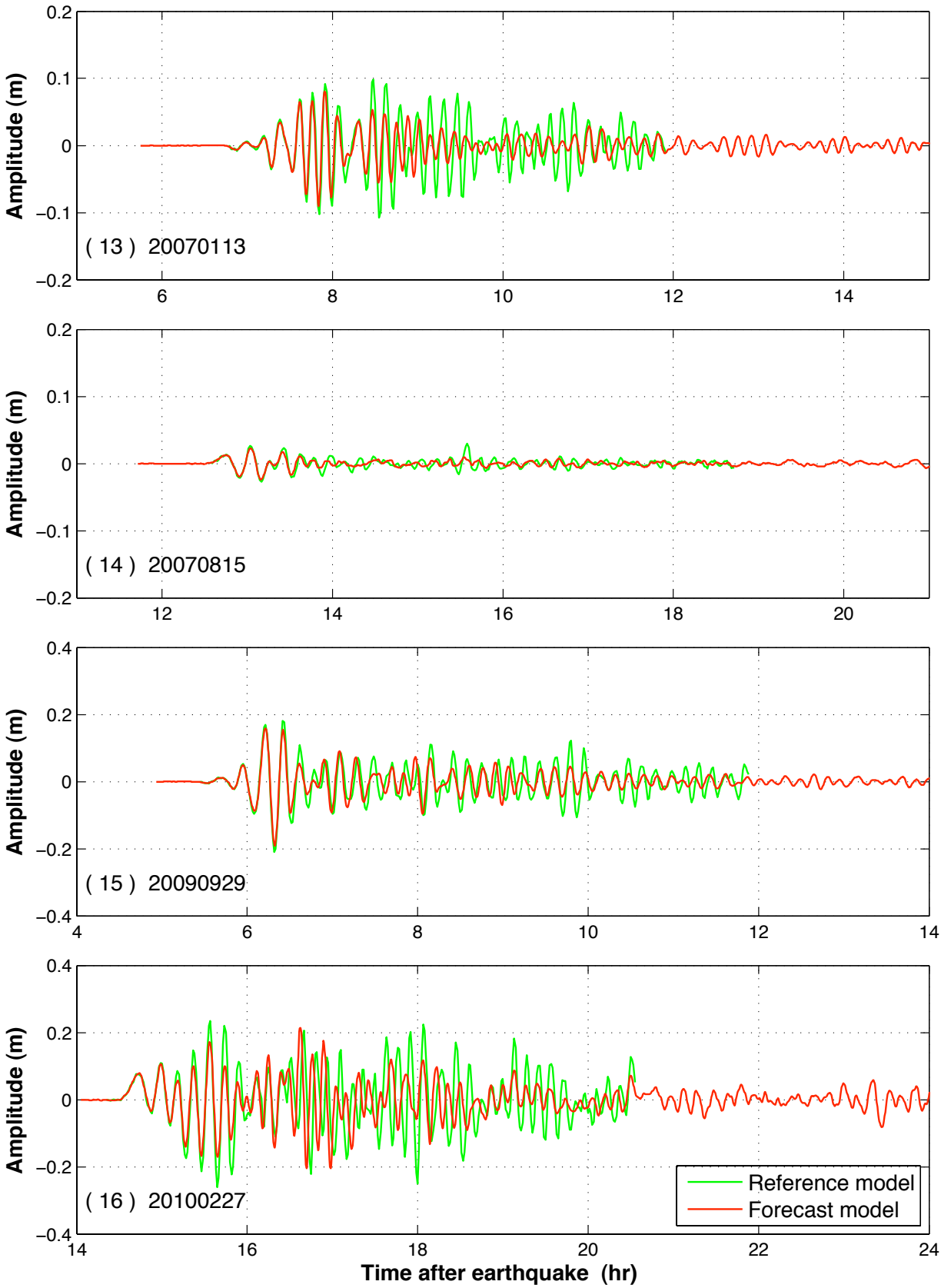
Amplitude (m)
(13) 20070113
(14) 20070815
(15) 20090929
(16) 20100227
Reference model
Forecast model
Time after earthquake (hr)

Figure 10 Modeled time series of wave amplitudes at Keauhou warning point for the past 17 tsunamis.

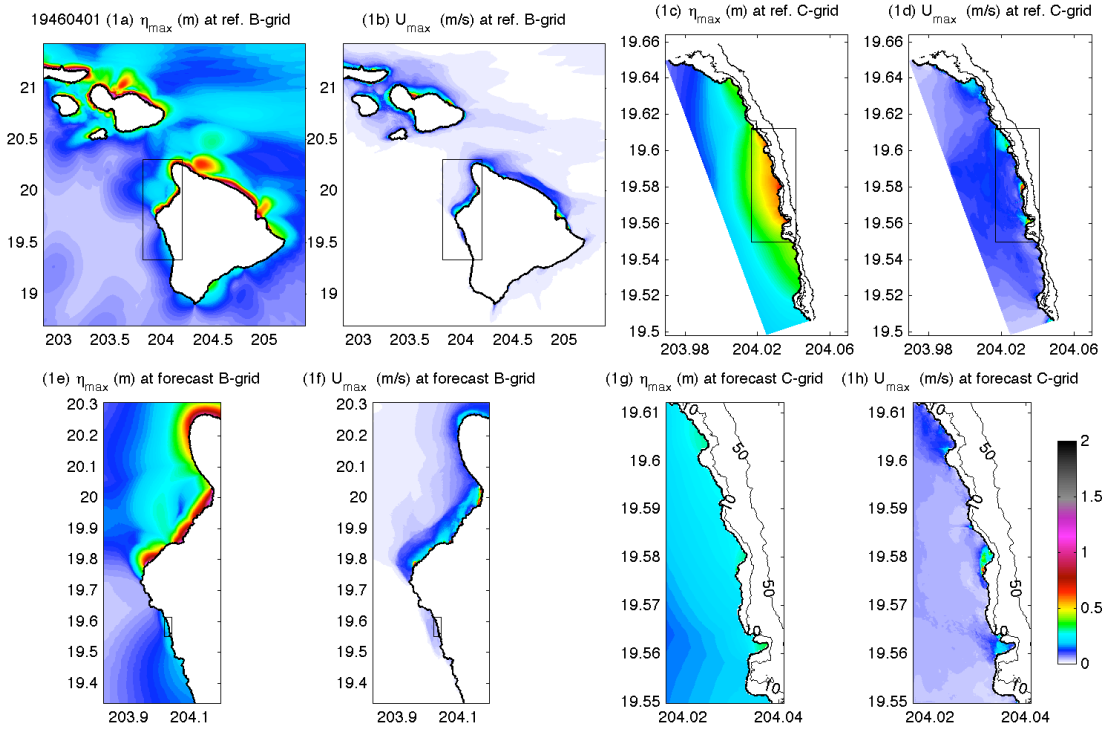
19460401 (1a) η_{max} (m) at ref. B-grid
(1b) U_{max} (m/s) at ref. B-grid
(1c) η_{max} (m) at ref. C-grid
(1d) U_{max} (m/s) at ref. C-grid
(1e) η_{max} (m) at forecast B-grid
(1f) U_{max} (m/s) at forecast B-grid
(1g) η_{max} (m) at forecast C-grid
(1h) U_{max} (m/s) at forecast C-grid

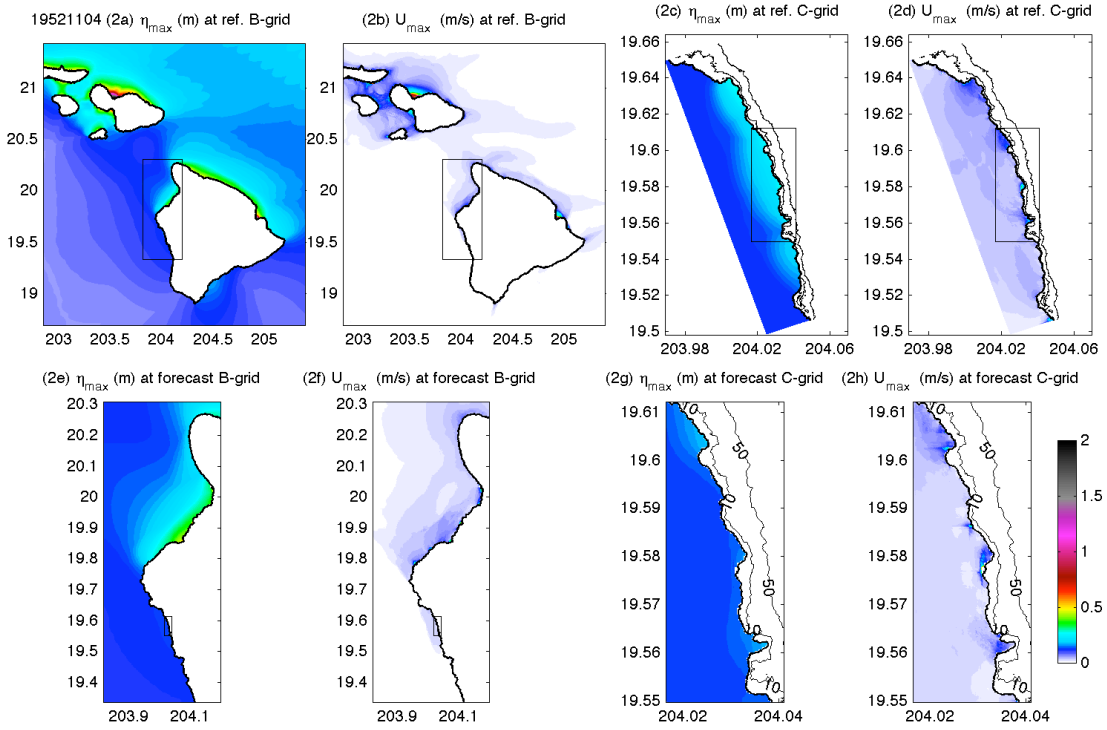
19521104 (2a) η_{max} (m) at ref. B-grid
(2b) U_{max} (m/s) at ref. B-grid
(2c) η_{max} (m) at ref. C-grid
(2d) U_{max} (m/s) at ref. C-grid
(2e) η_{max} (m) at forecast B-grid
(2f) U_{max} (m/s) at forecast B-grid
(2g) η_{max} (m) at forecast C-grid
(2h) U_{max} (m/s) at forecast C-grid

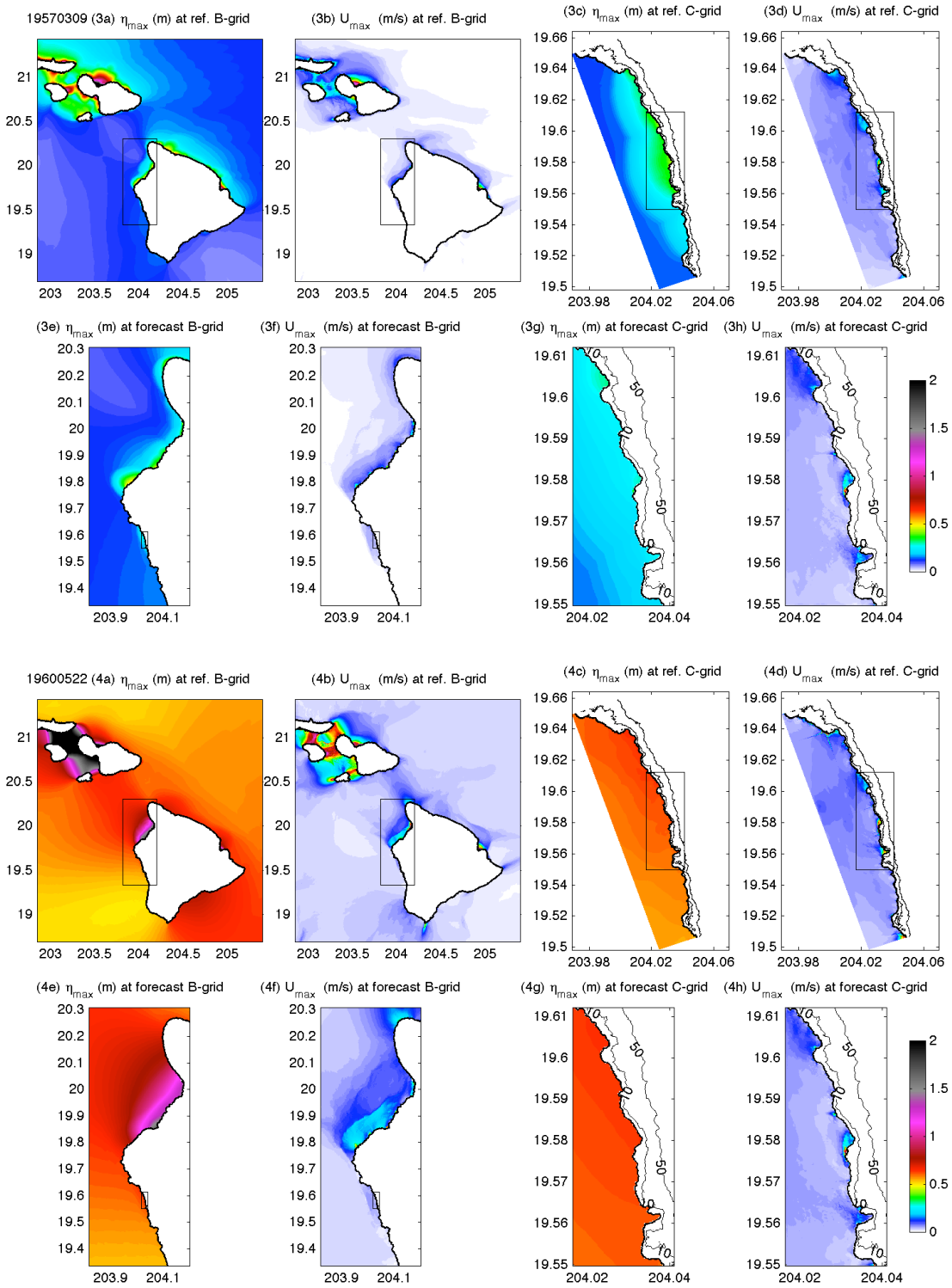
19570309 (3a) η_{max} (m) at ref. B-grid
(3b) U_{max} (m/s) at ref. B-grid
(3c) η_{max} (m) at ref. C-grid
(3d) U_{max} (m/s) at ref. C-grid
(3e) η_{max} (m) at forecast B-grid
(3f) U_{max} (m/s) at forecast B-grid
(3g) η_{max} (m) at forecast C-grid
(3h) U_{max} (m/s) at forecast C-grid
19600522 (4a) η_{max} (m) at ref. B-grid
(4b) U_{max} (m/s) at ref. B-grid
(4c) η_{max} (m) at ref. C-grid
(4d) U_{max} (m/s) at ref. C-grid
(4e) η_{max} (m) at forecast B-grid
(4f) U_{max} (m/s) at forecast B-grid
(4g) η_{max} (m) at forecast C-grid
(4h) U_{max} (m/s) at forecast C-grid

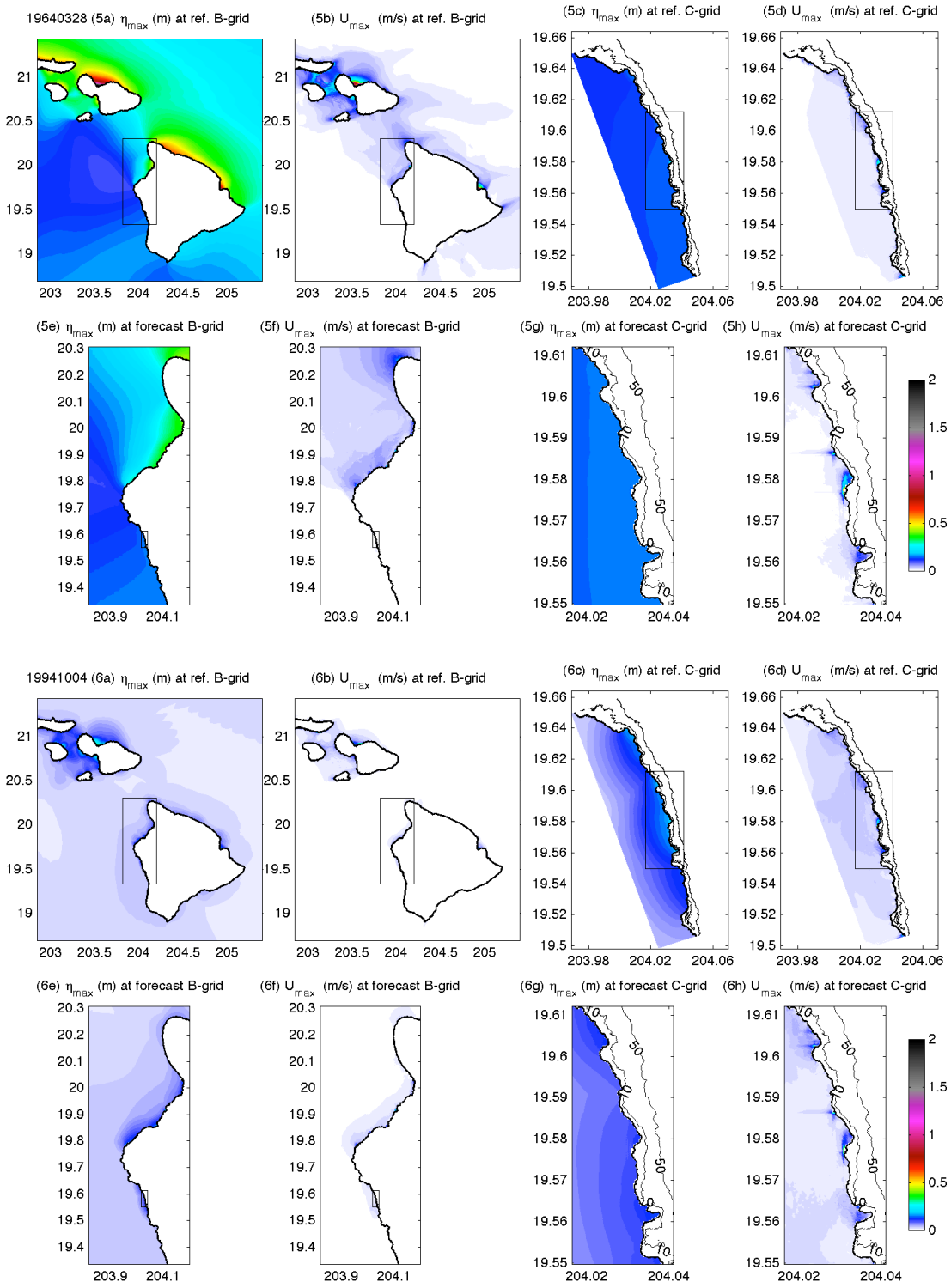
19640328 (5a) η_{max} (m) at ref. B-grid
(5b) U_{max} (m/s) at ref. B-grid
(5c) η_{max} (m) at ref. C-grid
(5d) U_{max} (m/s) at ref. C-grid
(5e) η_{max} (m) at forecast B-grid
(5f) U_{max} (m/s) at forecast B-grid
(5g) η_{max} (m) at forecast C-grid
(5h) U_{max} (m/s) at forecast C-grid
19941004 (6a) η_{max} (m) at ref. B-grid
(6b) U_{max} (m/s) at ref. B-grid
(6c) η_{max} (m) at ref. C-grid
(6d) U_{max} (m/s) at ref. C-grid
(6e) η_{max} (m) at forecast B-grid
(6f) U_{max} (m/s) at forecast B-grid
(6g) η_{max} (m) at forecast C-grid
(6h) U_{max} (m/s) at forecast C-grid

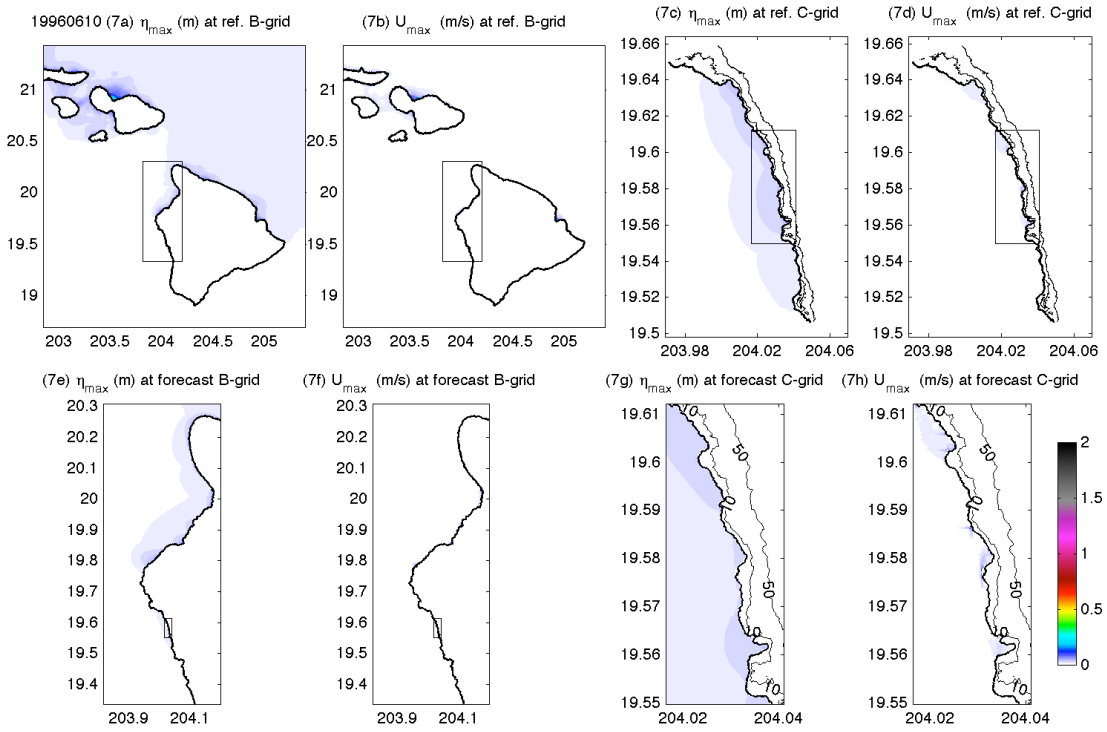
19960610 (7a) η_{max} (m) at ref. B-grid
(7b) U_{max} (m/s) at ref. B-grid
(7c) η_{max} (m) at ref. C-grid
(7d) U_{max} (m/s) at ref. C-grid
(7e) η_{max} (m) at forecast B-grid
(7f) U_{max} (m/s) at forecast B-grid
(7g) η_{max} (m) at forecast C-grid
(7h) U_{max} (m/s) at forecast C-grid

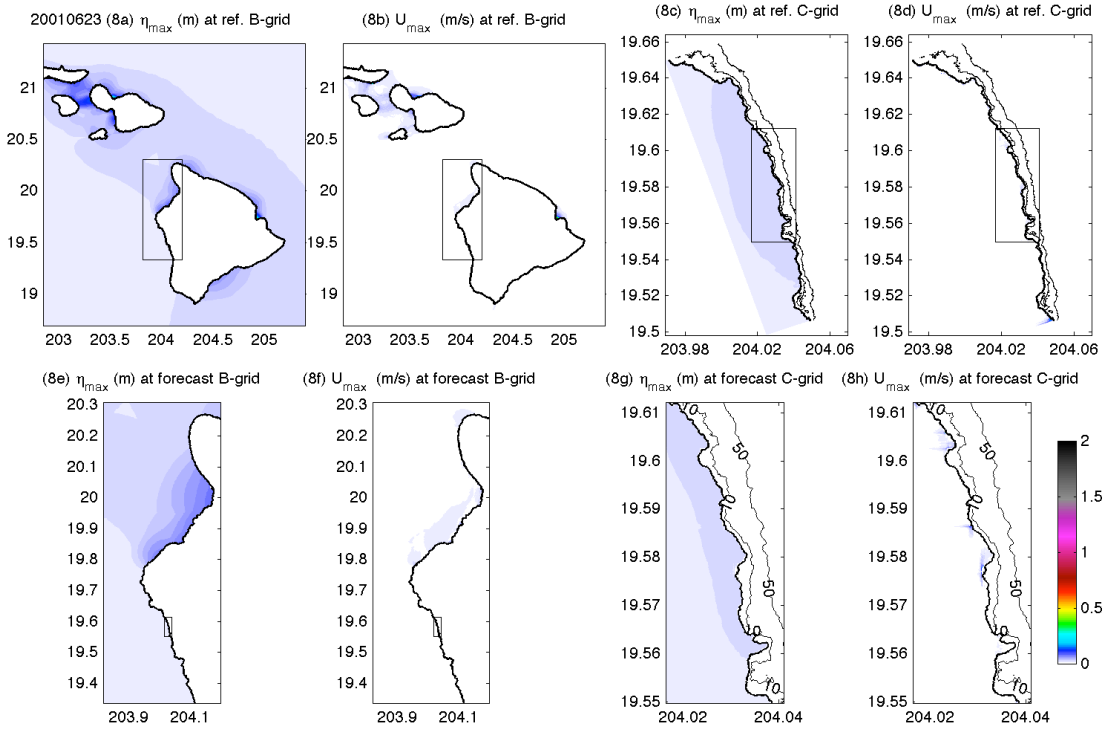
20010623 (8a) η_{max} (m) at ref. B-grid
(8b) U_{max} (m/s) at ref. B-grid
(8c) η_{max} (m) at ref. C-grid
(8d) U_{max} (m/s) at ref. C-grid
(8e) η_{max} (m) at forecast B-grid
(8f) U_{max} (m/s) at forecast B-grid
(8g) η_{max} (m) at forecast C-grid
(8h) U_{max} (m/s) at forecast C-grid

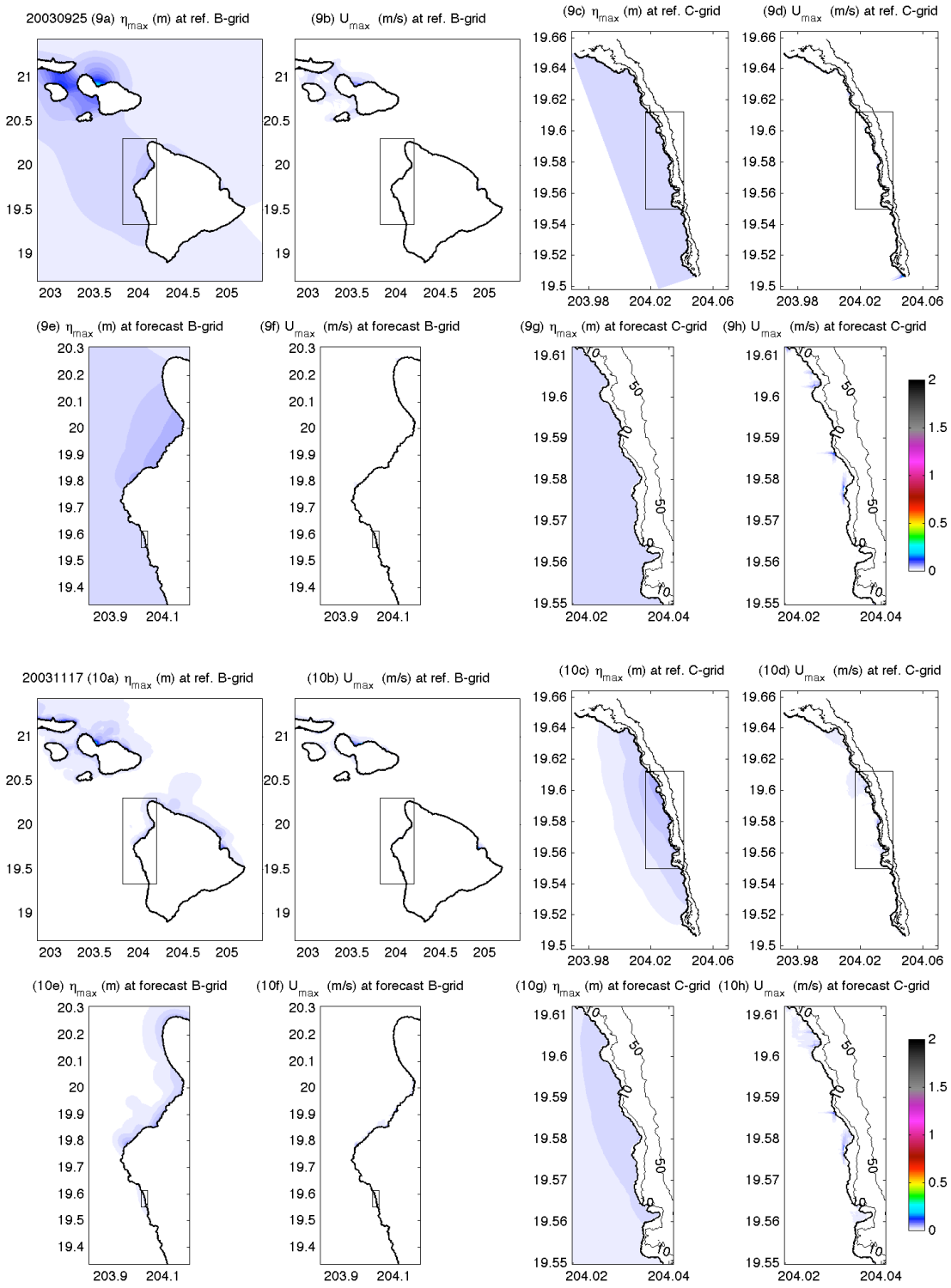
20030925 (9a) η_{max} (m) at ref. B-grid
(9b) U_{max} (m/s) at ref. B-grid
(9c) η_{max} (m) at ref. C-grid
(9d) U_{max} (m/s) at ref. C-grid
(9e) η_{max} (m) at forecast B-grid
(9f) U_{max} (m/s) at forecast B-grid
(9g) η_{max} (m) at forecast C-grid
(9h) U_{max} (m/s) at forecast C-grid
20031117 (10a) η_{max} (m) at ref. B-grid
(10b) U_{max} (m/s) at ref. B-grid
(10c) η_{max} (m) at ref. C-grid
(10d) U_{max} (m/s) at ref. C-grid
(10e) η_{max} (m) at forecast B-grid
(10f) U_{max} (m/s) at forecast B-grid
(10g) η_{max} (m) at forecast C-grid
(10h) U_{max} (m/s) at forecast C-grid

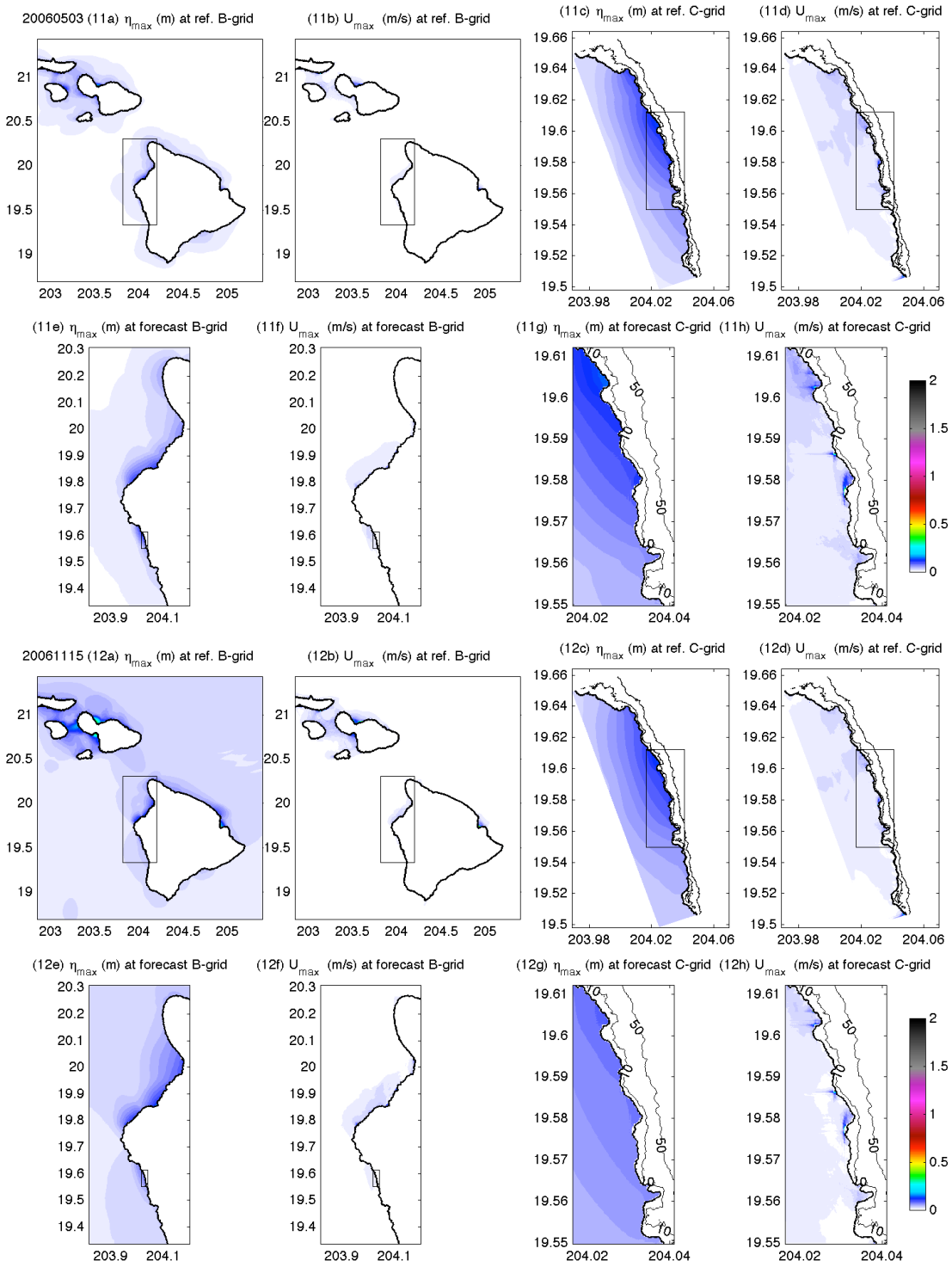
20060503 (11a) η_{max} (m) at ref. B-grid
(11b) U_{max} (m/s) at ref. B-grid
(11c) η_{max} (m) at ref. C-grid
(11d) U_{max} (m/s) at ref. C-grid
(11e) η_{max} (m) at forecast B-grid
(11f) U_{max} (m/s) at forecast B-grid
(11g) η_{max} (m) at forecast C-grid
(11h) U_{max} (m/s) at forecast C-grid
20061115 (12a) η_{max} (m) at ref. B-grid
(12b) U_{max} (m/s) at ref. B-grid
(12c) η_{max} (m) at ref. C-grid
(12d) U_{max} (m/s) at ref. C-grid
(12e) η_{max} (m) at forecast B-grid
(12f) U_{max} (m/s) at forecast B-grid
(12g) η_{max} (m) at forecast C-grid
(12h) U_{max} (m/s) at forecast C-grid

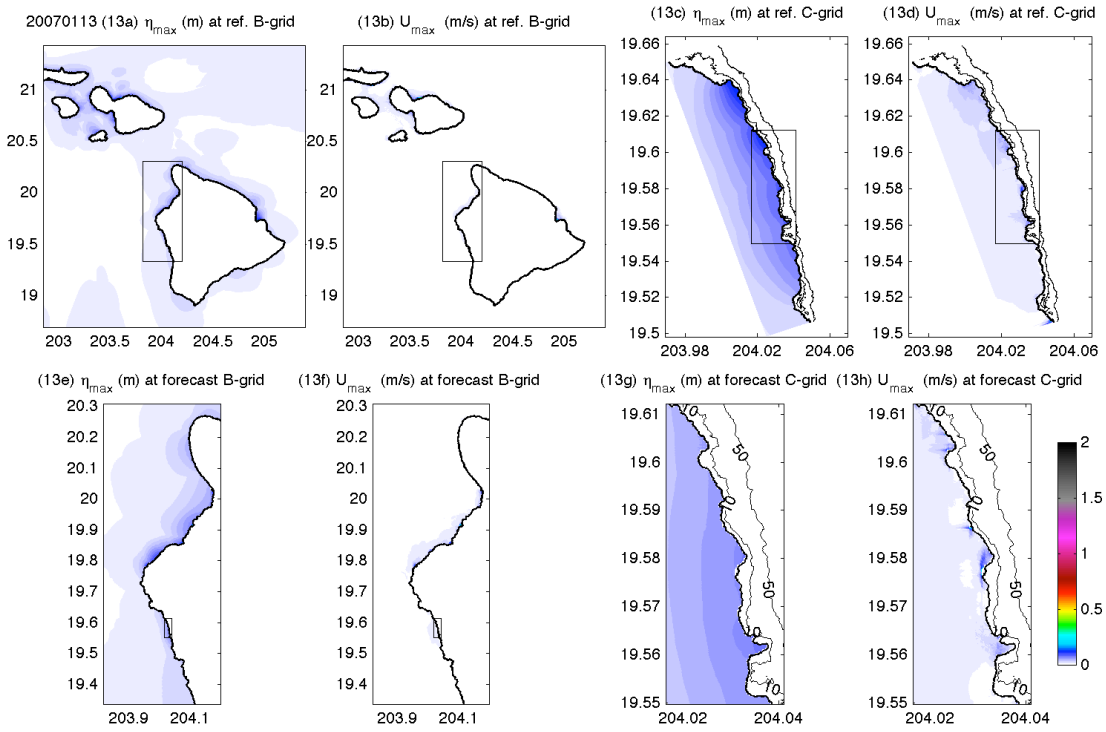
20070113 (13a) η_{max} (m) at ref. B-grid
(13b) U_{max} (m/s) at ref. B-grid
(13c) η_{max} (m) at ref. C-grid
(13d) U_{max} (m/s) at ref. C-grid
(13e) η_{max} (m) at forecast B-grid
(13f) U_{max} (m/s) at forecast B-grid
(13g) η_{max} (m) at forecast C-grid
(13h) U_{max} (m/s) at forecast C-grid

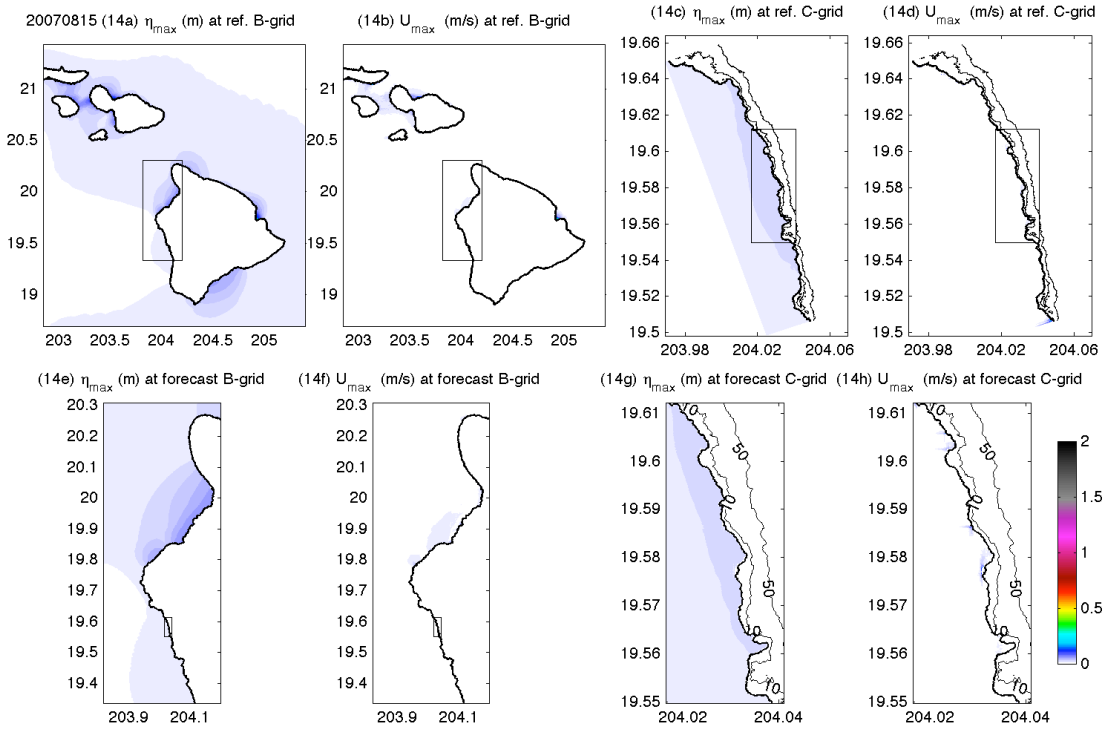
20070815 (14a) η_{max} (m) at ref. B-grid
(14b) U_{max} (m/s) at ref. B-grid
(14c) η_{max} (m) at ref. C-grid
(14d) U_{max} (m/s) at ref. C-grid
(14e) η_{max} (m) at forecast B-grid
(14f) U_{max} (m/s) at forecast B-grid
(14g) η_{max} (m) at forecast C-grid
(14h) U_{max} (m/s) at forecast C-grid

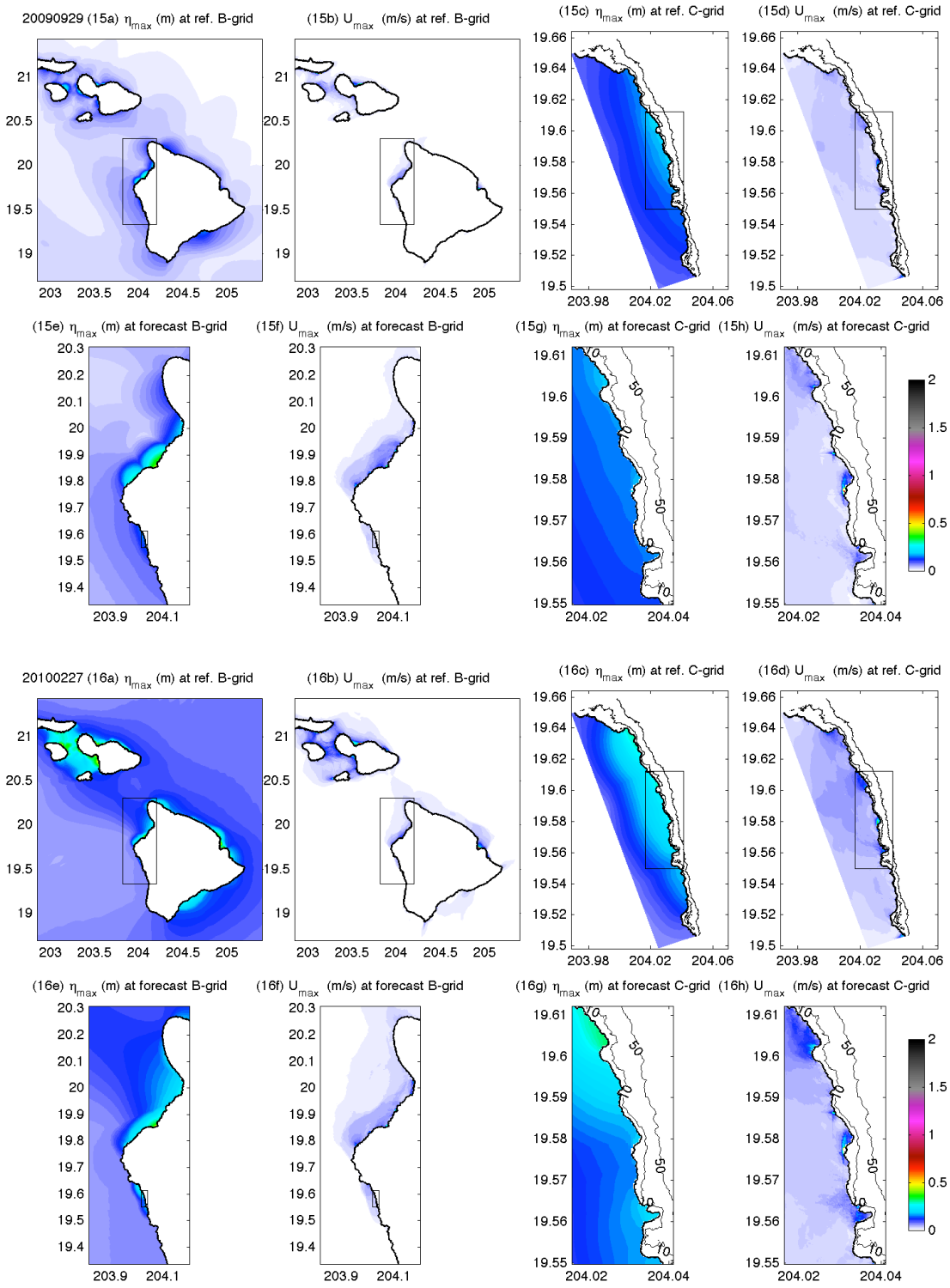
20090929 (15a) η_{max} (m) at ref. B-grid
(15b) U_{max} (m/s) at ref. B-grid
(15c) η_{max} (m) at ref. C-grid
(15d) U_{max} (m/s) at ref. C-grid
(15e) η_{max} (m) at forecast B-grid
(15f) U_{max} (m/s) at forecast B-grid
(15g) η_{max} (m) at forecast C-grid
(15h) U_{max} (m/s) at forecast C-grid
20100227 (16a) η_{max} (m) at ref. B-grid
(16b) U_{max} (m/s) at ref. B-grid
(16c) η_{max} (m) at ref. C-grid
(16d) U_{max} (m/s) at ref. C-grid
(16e) η_{max} (m) at forecast B-grid
(16f) U_{max} (m/s) at forecast B-grid
(16g) η_{max} (m) at forecast C-grid
(16h) U_{max} (m/s) at forecast C-grid

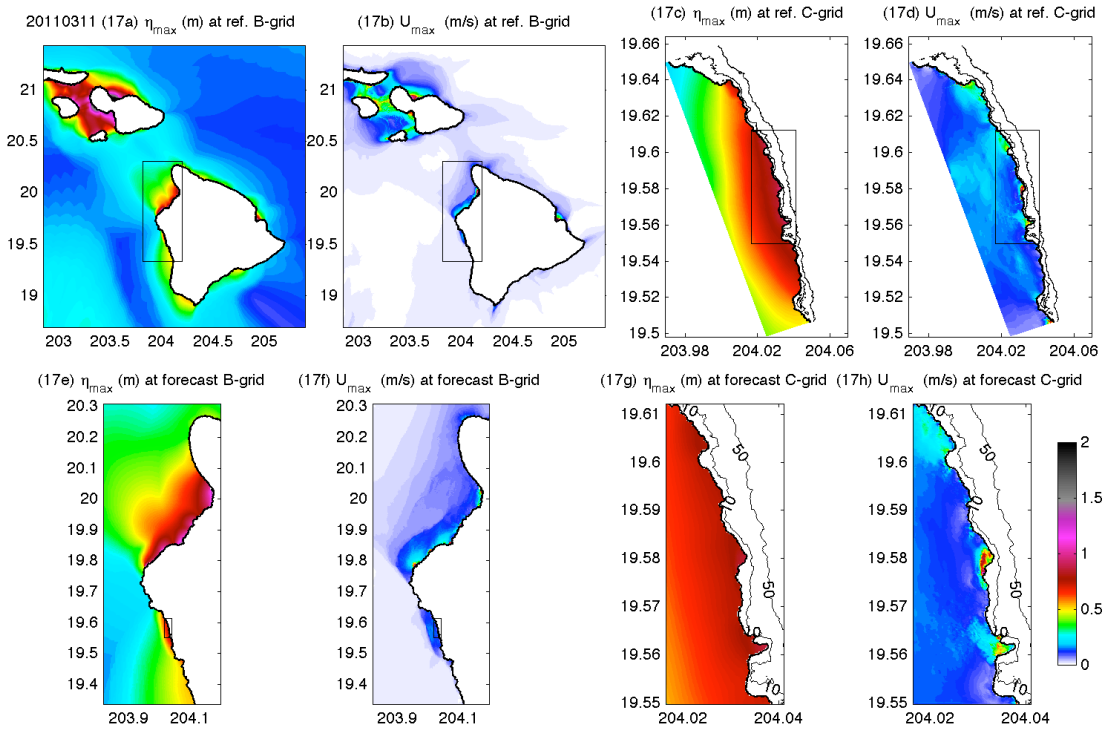

Figure 11 Computed maximum amplitude and current by the Keauhou (a, b, c and d) reference model and (e, f, g and h) forecast model for the sixteen past tsunamis.

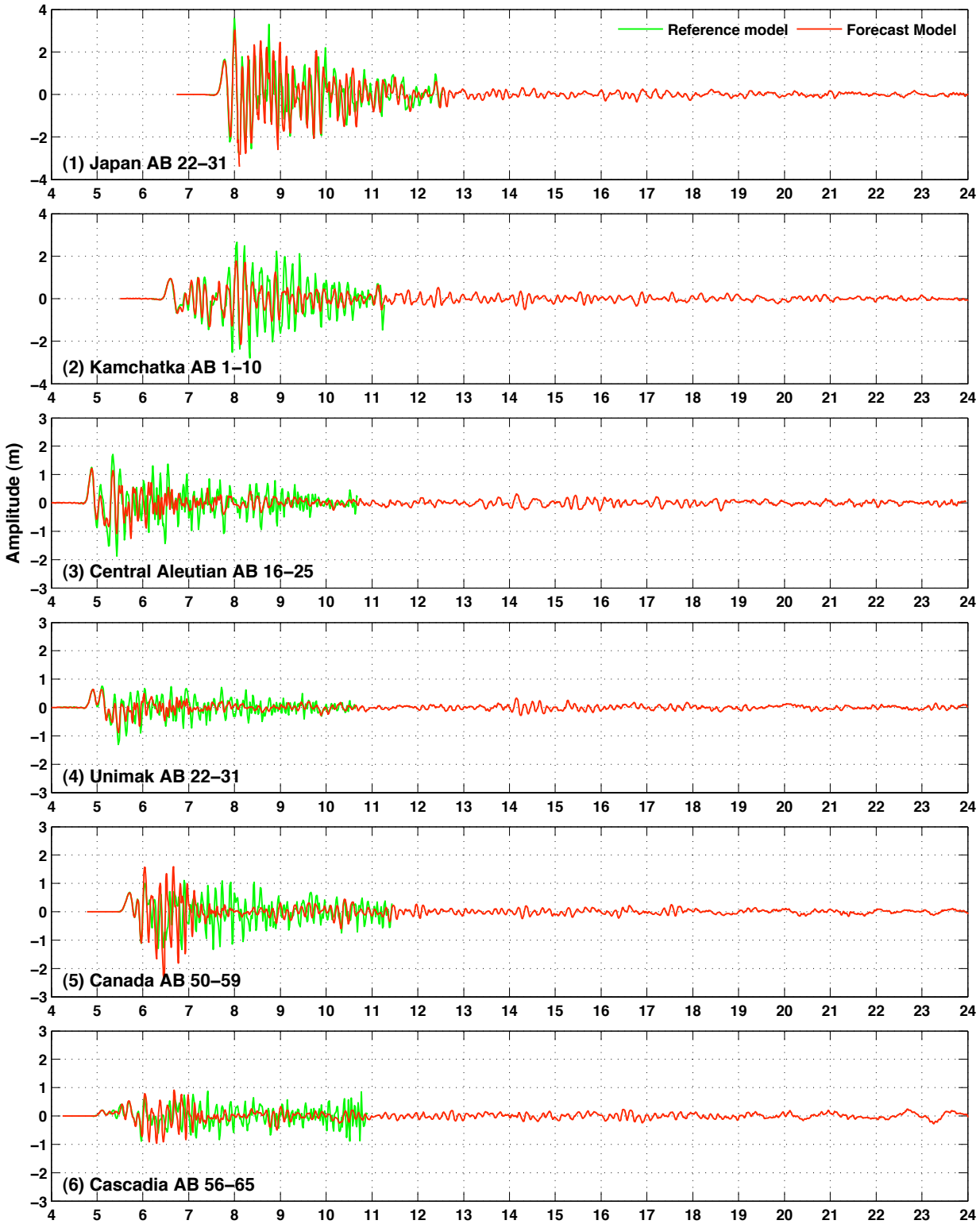
Reference model
Forecast Model
Amplitude (m)
(1) Japan AB 22–31
(2) Kamchatka AB 1–10
(3) Central Aleutian AB 16–25
(4) Unimak AB 22–31
(5) Canada AB 50–59
(6) Cascadia AB 56–65

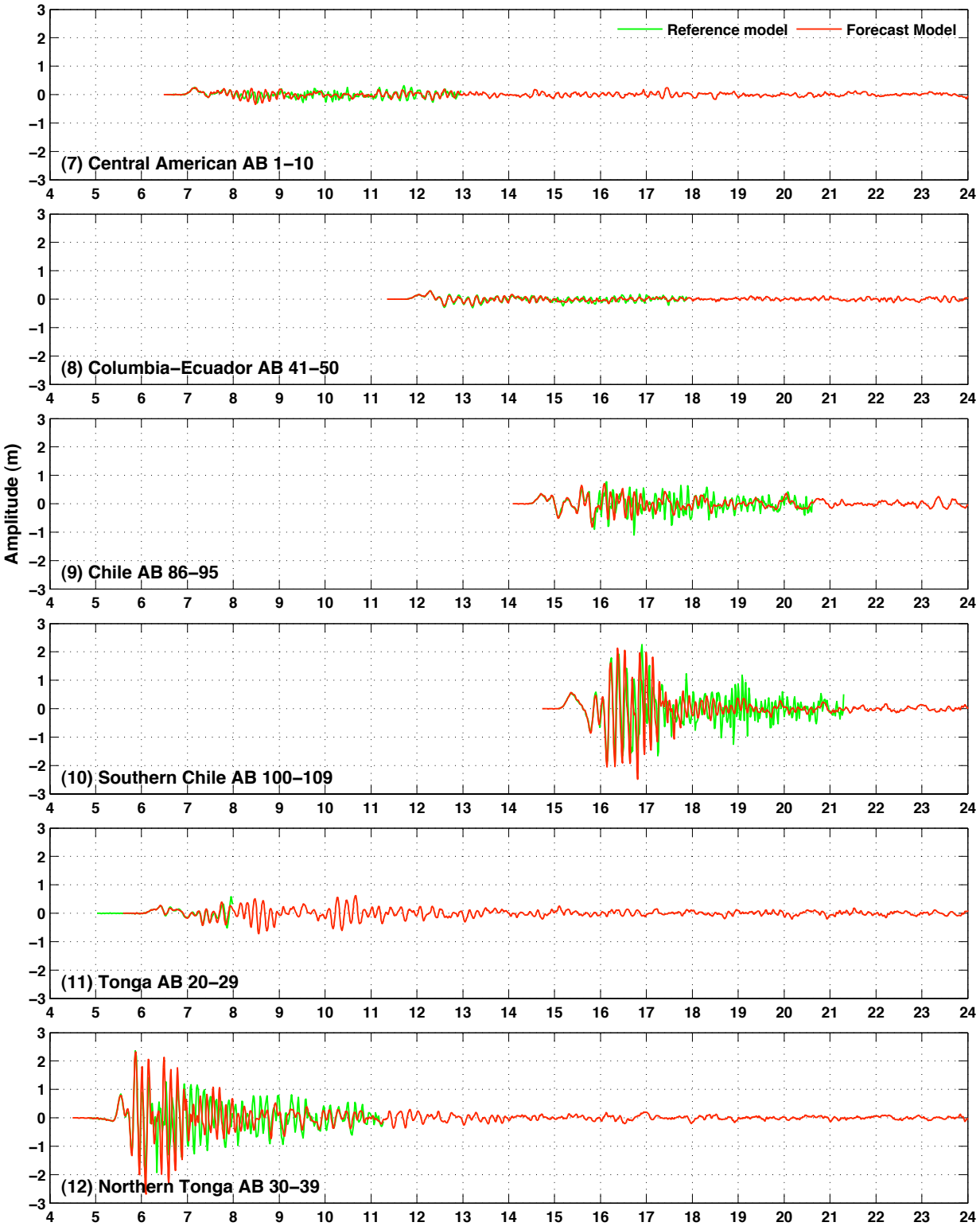
Reference model
Forecast Model
Amplitude (m)
(7) Central American AB 1–10
(8) Columbia–Ecuador AB 41–50
(9) Chile AB 86–95
(10) Southern Chile AB 100–109
(11) Tonga AB 20–29
(12) Northern Tonga AB 30–39

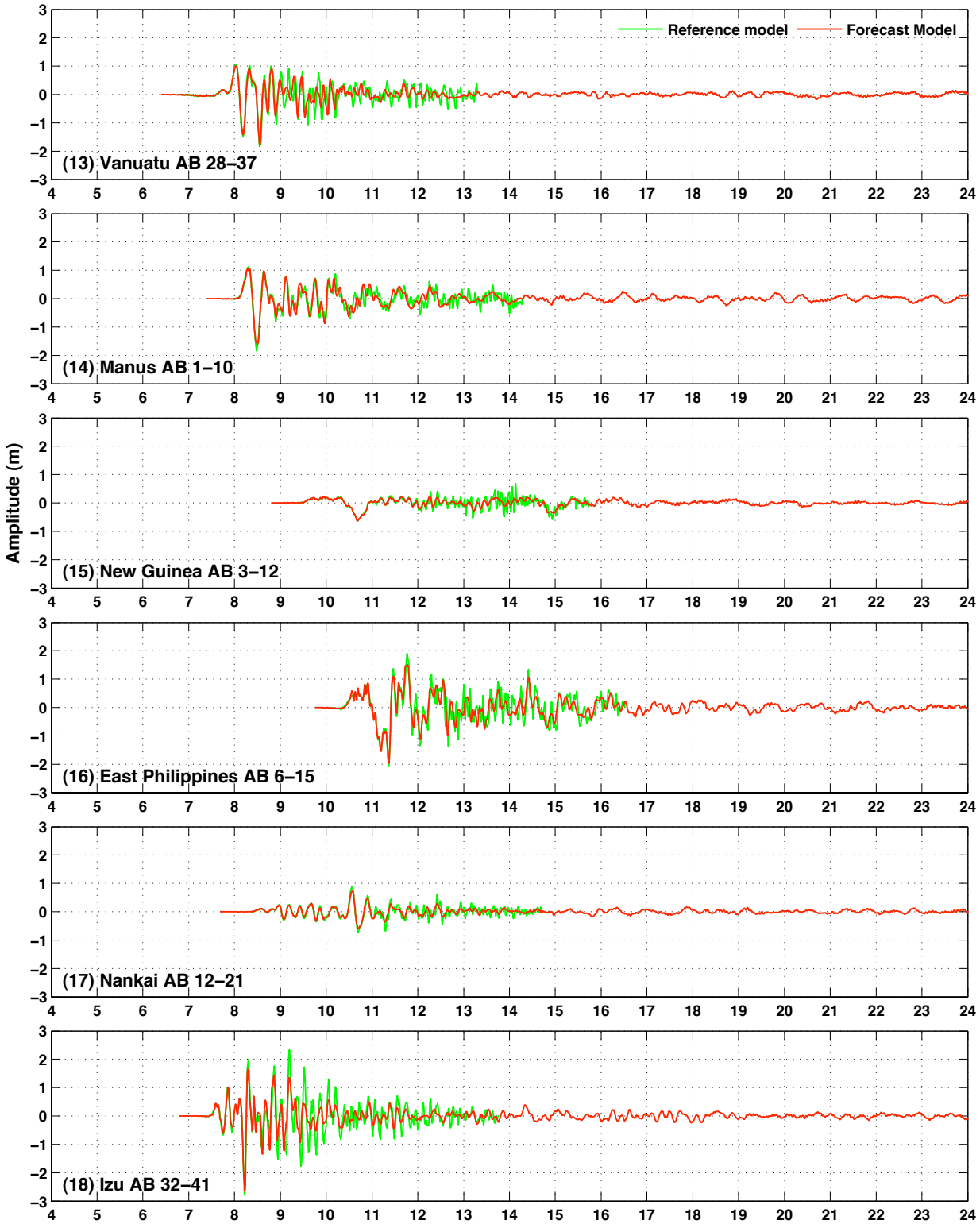

Figure 12 Modeled time series of wave amplitudes at Keauhou warning point for the eighteen simulated magnitude 9.3 tsunamis.

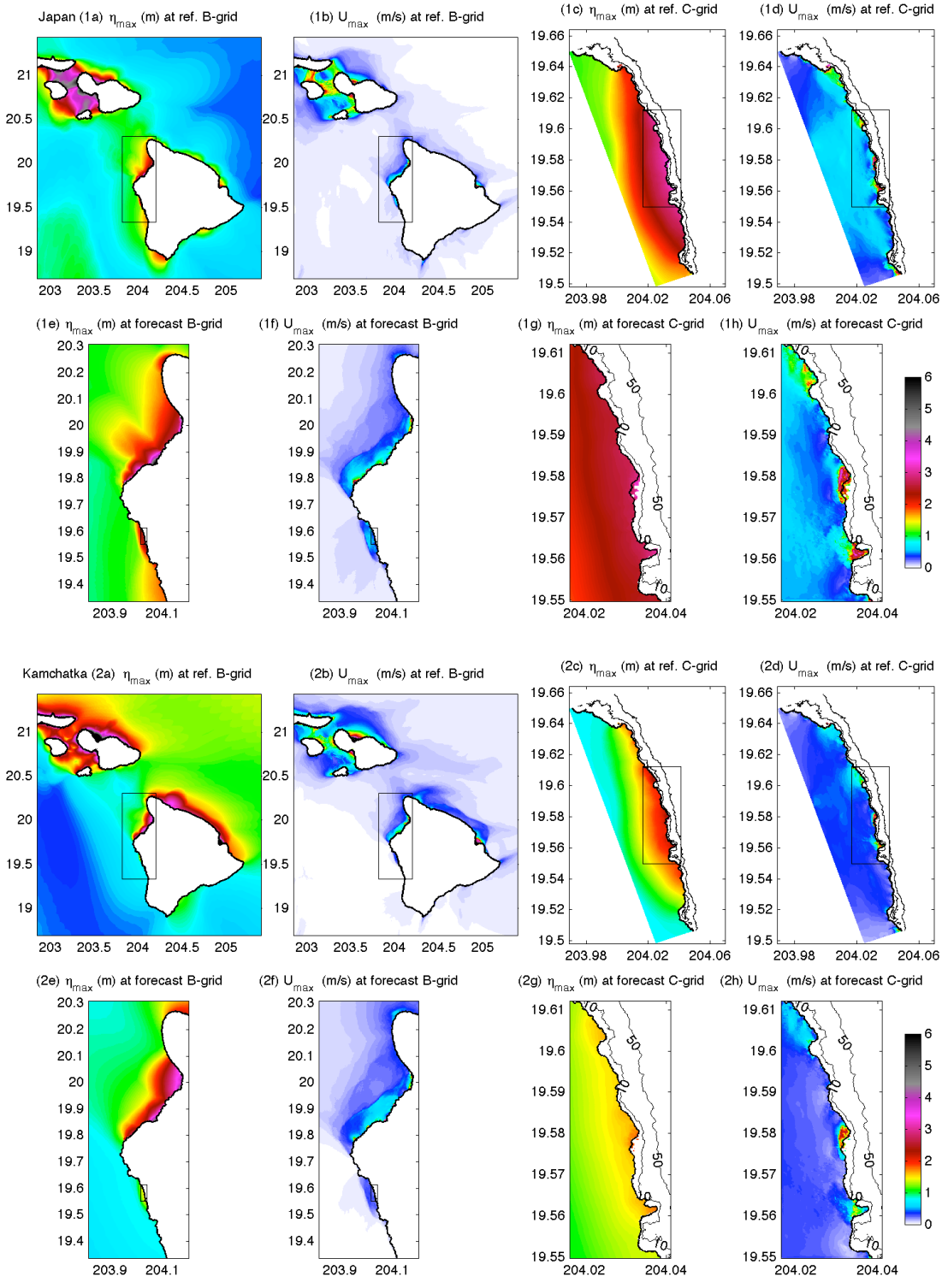
Japan (1a) η_{max} (m) at ref. B-grid
(1b) U_{max} (m/s) at ref. B-grid
(1c) η_{max} (m) at ref. C-grid
(1d) U_{max} (m/s) at ref. C-grid
(1e) η_{max} (m) at forecast B-grid
(1f) U_{max} (m/s) at forecast B-grid
(1g) η_{max} (m) at forecast C-grid
(1h) U_{max} (m/s) at forecast C-grid
Kamchatka (2a) η_{max} (m) at ref. B-grid
(2b) U_{max} (m/s) at ref. B-grid
(2c) η_{max} (m) at ref. C-grid
(2d) U_{max} (m/s) at ref. C-grid
(2e) η_{max} (m) at forecast B-grid
(2f) U_{max} (m/s) at forecast B-grid
(2g) η_{max} (m) at forecast C-grid
(2h) U_{max} (m/s) at forecast C-grid

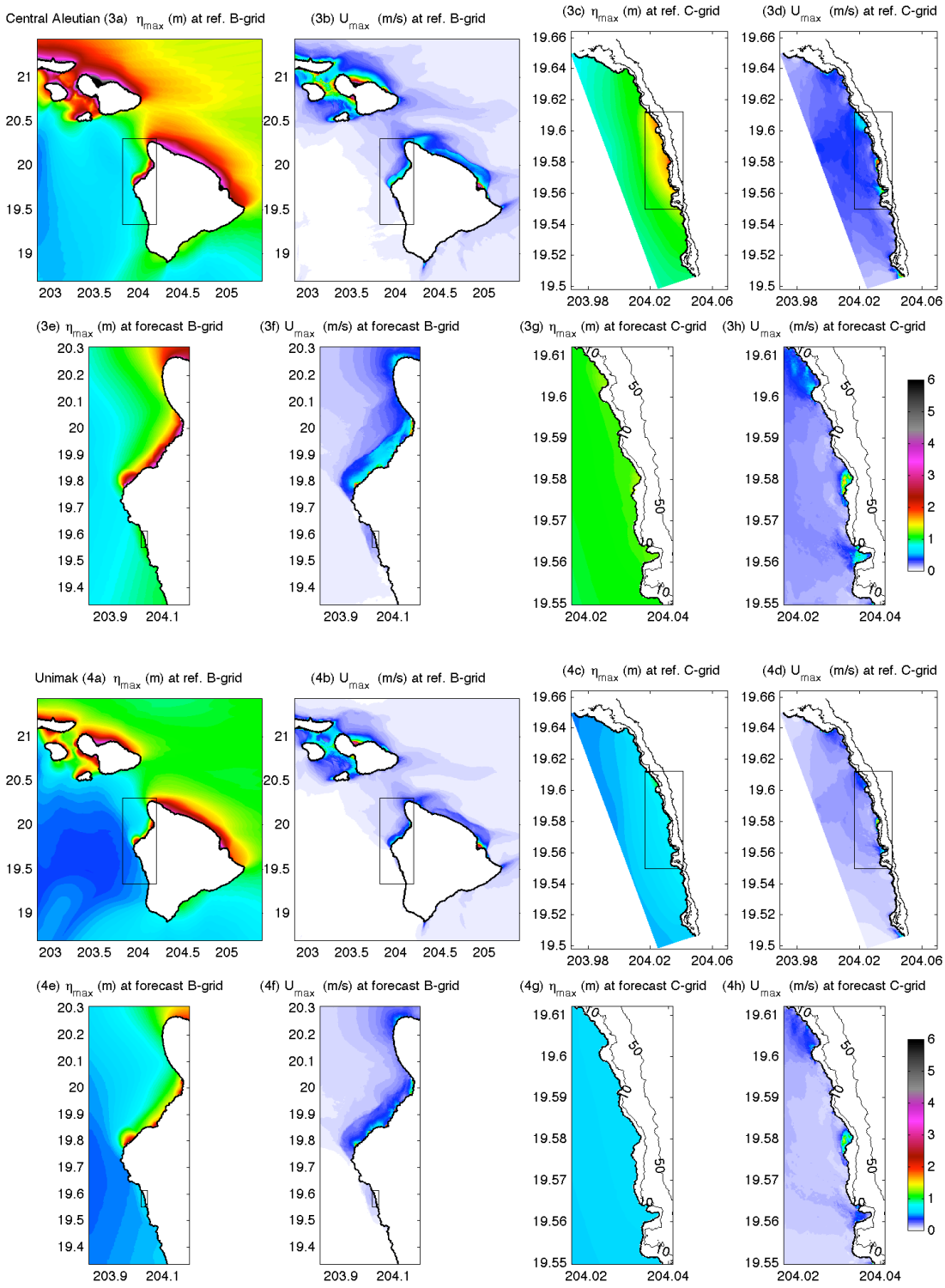
Central Aleutian (3a) η_{max} (m) at ref. B-grid
(3b) U_{max} (m/s) at ref. B-grid
(3c) η_{max} (m) at ref. C-grid
(3d) U_{max} (m/s) at ref. C-grid
(3e) η_{max} (m) at forecast B-grid
(3f) U_{max} (m/s) at forecast B-grid
(3g) η_{max} (m) at forecast C-grid
(3h) U_{max} (m/s) at forecast C-grid
Unimak (4a) η_{max} (m) at ref. B-grid
(4b) U_{max} (m/s) at ref. B-grid
(4c) η_{max} (m) at ref. C-grid
(4d) U_{max} (m/s) at ref. C-grid
(4e) η_{max} (m) at forecast B-grid
(4f) U_{max} (m/s) at forecast B-grid
(4g) η_{max} (m) at forecast C-grid
(4h) U_{max} (m/s) at forecast C-grid

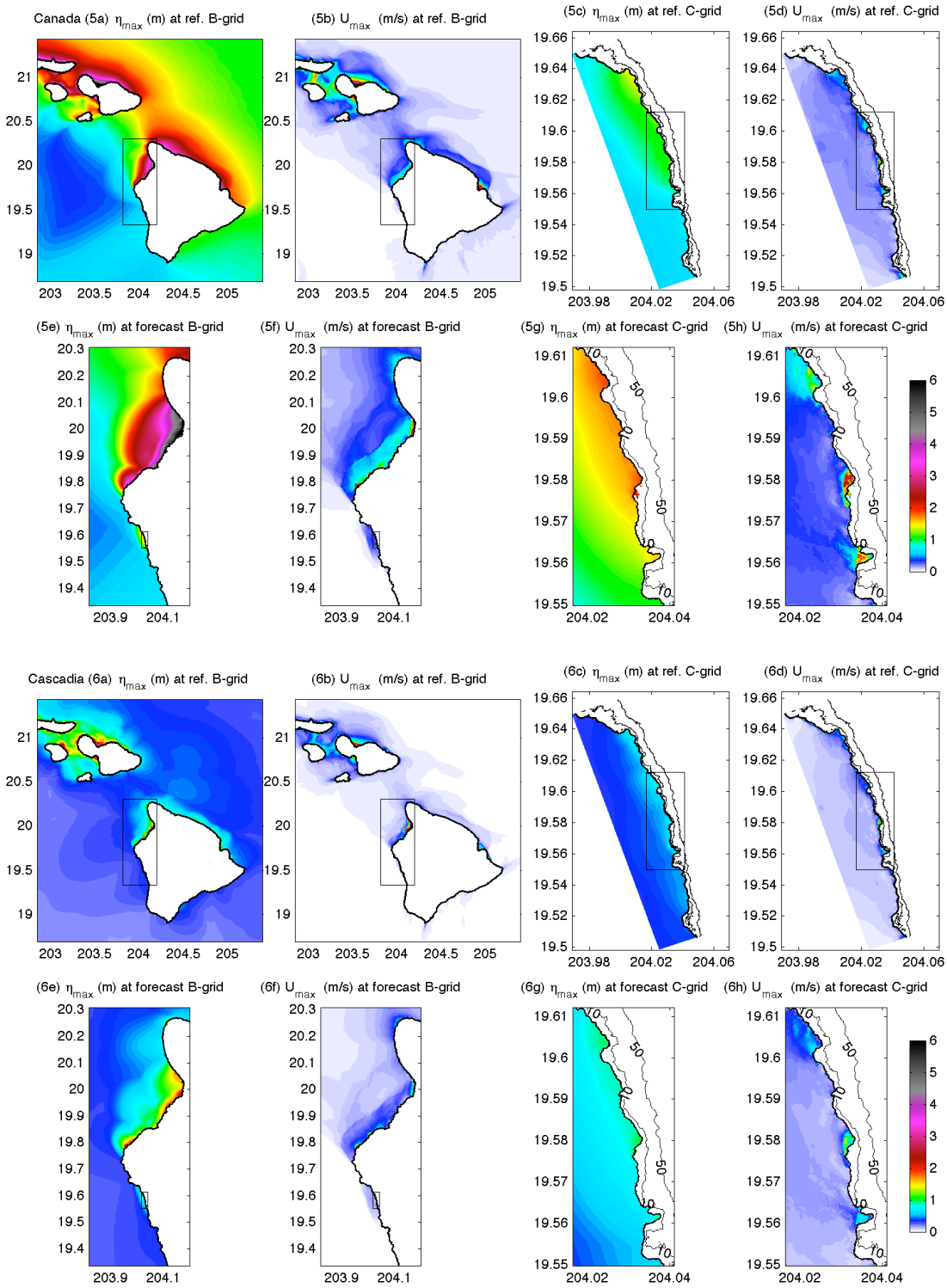
Canada (5a) η_{max} (m) at ref. B-grid
(5b) U_{max} (m/s) at ref. B-grid
(5c) η_{max} (m) at ref. C-grid
(5d) U_{max} (m/s) at ref. C-grid
(5e) η_{max} (m) at forecast B-grid
(5f) U_{max} (m/s) at forecast B-grid
(5g) η_{max} (m) at forecast C-grid
(5h) U_{max} (m/s) at forecast C-grid
Cascadia (6a) η_{max} (m) at ref. B-grid
(6b) U_{max} (m/s) at ref. B-grid
(6c) η_{max} (m) at ref. C-grid
(6d) U_{max} (m/s) at ref. C-grid
(6e) η_{max} (m) at forecast B-grid
(6f) U_{max} (m/s) at forecast B-grid
(6g) η_{max} (m) at forecast C-grid
(6h) U_{max} (m/s) at forecast C-grid

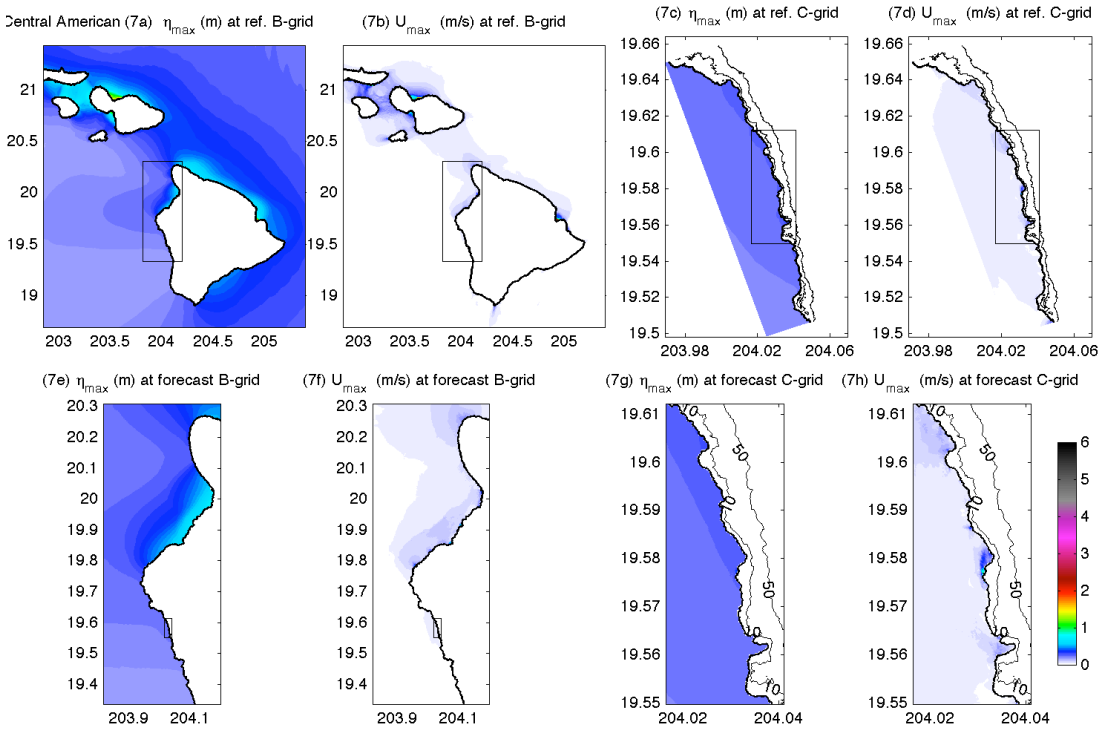
Central American (7a) η_{max} (m) at ref. B-grid
(7b) U_{max} (m/s) at ref. B-grid
(7c) η_{max} (m) at ref. C-grid
(7d) U_{max} (m/s) at ref. C-grid
(7e) η_{max} (m) at forecast B-grid
(7f) U_{max} (m/s) at forecast B-grid
(7g) η_{max} (m) at forecast C-grid
(7h) U_{max} (m/s) at forecast C-grid

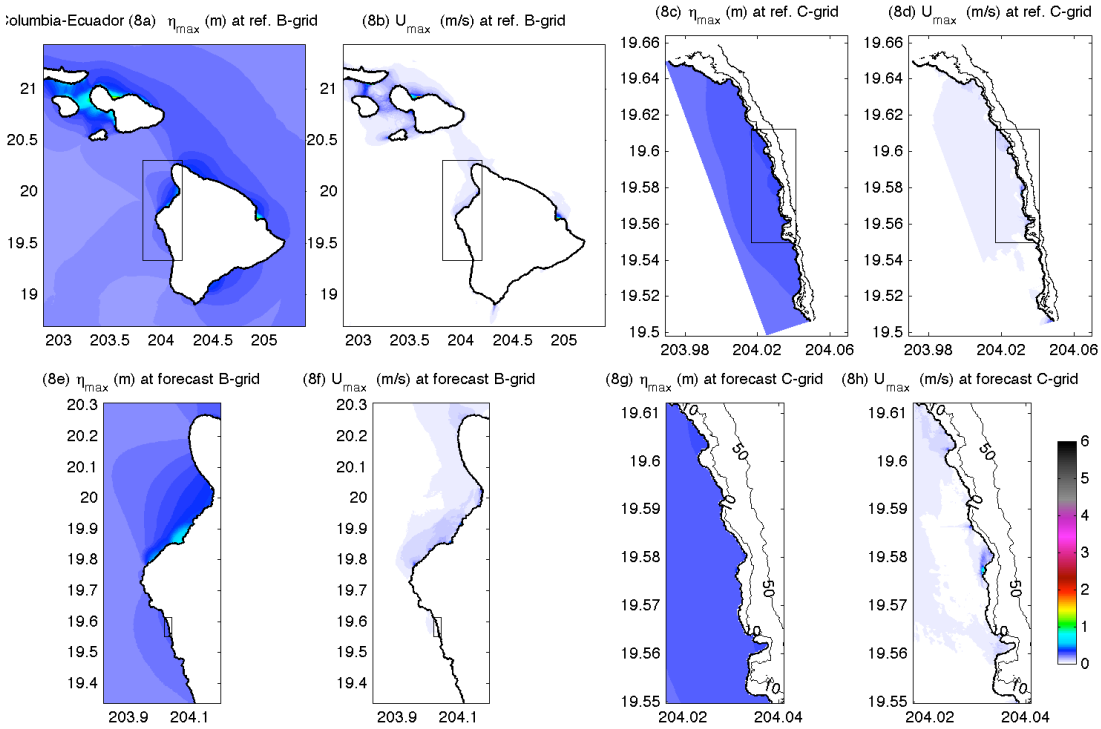
Columbia-Ecuador (8a) η_{max} (m) at ref. B-grid
(8b) U_{max} (m/s) at ref. B-grid
(8c) η_{max} (m) at ref. C-grid
(8d) U_{max} (m/s) at ref. C-grid
(8e) η_{max} (m) at forecast B-grid
(8f) U_{max} (m/s) at forecast B-grid
(8g) η_{max} (m) at forecast C-grid
(8h) U_{max} (m/s) at forecast C-grid

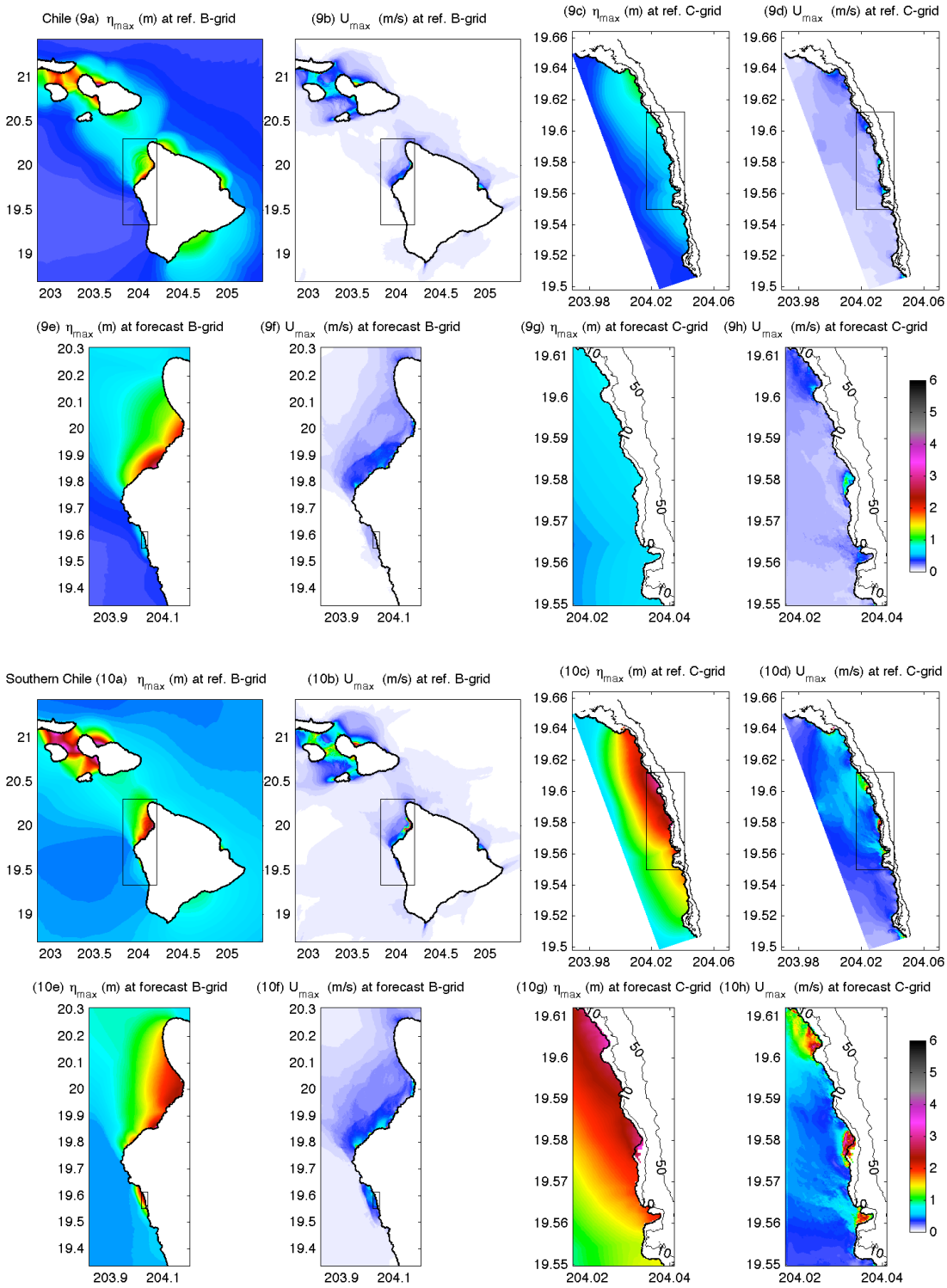
Chile (9a) ηmax (m) at ref. B-grid
(9b) Umax (m/s) at ref. B-grid
(9c) ηmax (m) at ref. C-grid
(9d) Umax (m/s) at ref. C-grid
(9e) ηmax (m) at forecast B-grid
(9f) Umax (m/s) at forecast B-grid
(9g) ηmax (m) at forecast C-grid
(9h) Umax (m/s) at forecast C-grid
Southern Chile (10a) ηmax (m) at ref. B-grid
(10b) Umax (m/s) at ref. B-grid
(10c) ηmax (m) at ref. C-grid
(10d) Umax (m/s) at ref. C-grid
(10e) ηmax (m) at forecast B-grid
(10f) Umax (m/s) at forecast B-grid
(10g) ηmax (m) at forecast C-grid
(10h) Umax (m/s) at forecast C-grid

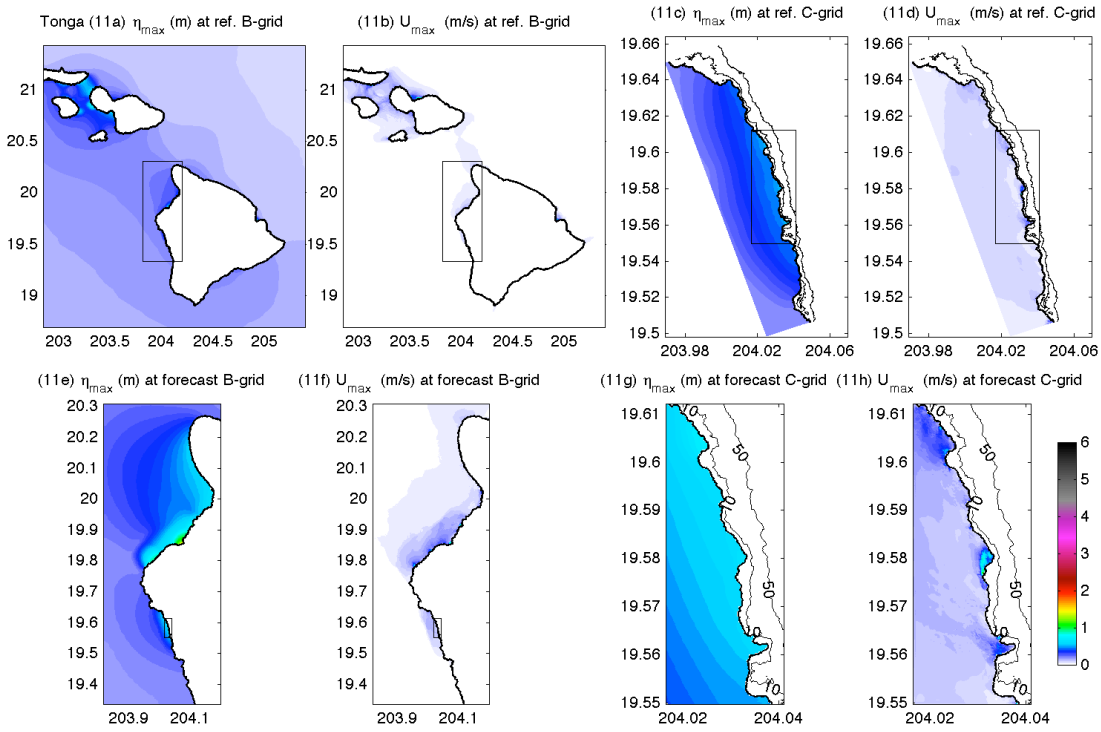
Tonga (11a) η_{max} (m) at ref. B-grid
(11b) U_{max} (m/s) at ref. B-grid
(11c) η_{max} (m) at ref. C-grid
(11d) U_{max} (m/s) at ref. C-grid
(11e) η_{max} (m) at forecast B-grid
(11f) U_{max} (m/s) at forecast B-grid
(11g) η_{max} (m) at forecast C-grid
(11h) U_{max} (m/s) at forecast C-grid

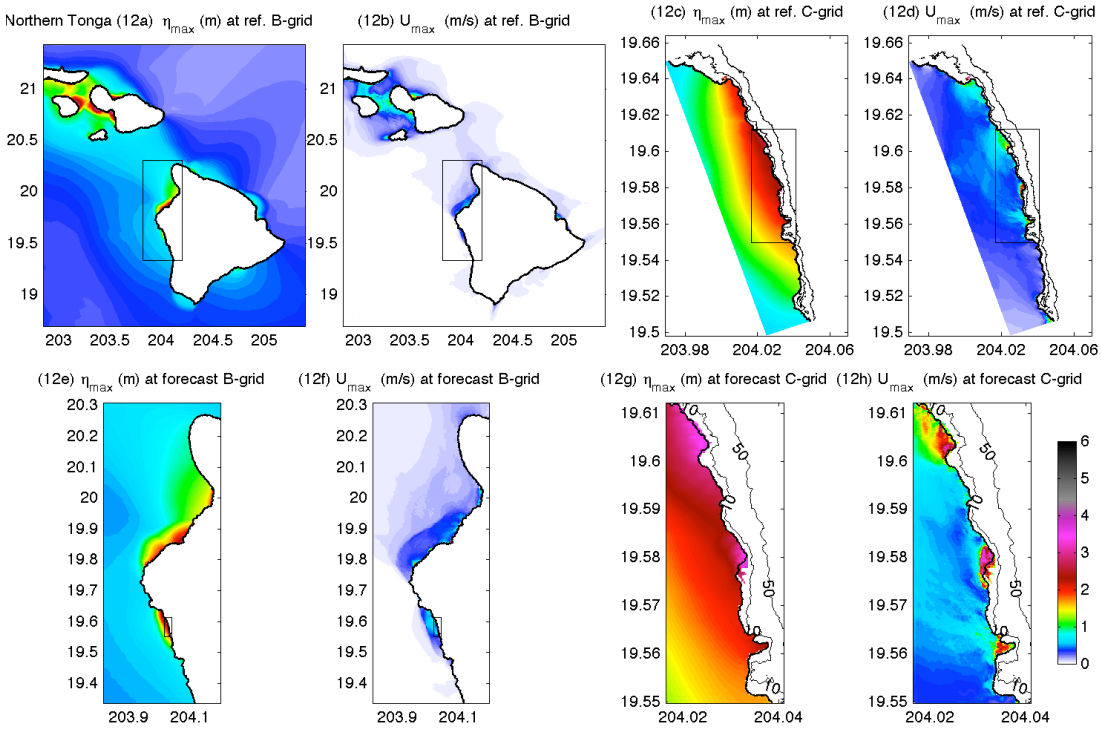
Northern Tonga (12a) η_{max} (m) at ref. B-grid
(12b) U_{max} (m/s) at ref. B-grid
(12c) η_{max} (m) at ref. C-grid
(12d) U_{max} (m/s) at ref. C-grid
(12e) η_{max} (m) at forecast B-grid
(12f) U_{max} (m/s) at forecast B-grid
(12g) η_{max} (m) at forecast C-grid
(12h) U_{max} (m/s) at forecast C-grid

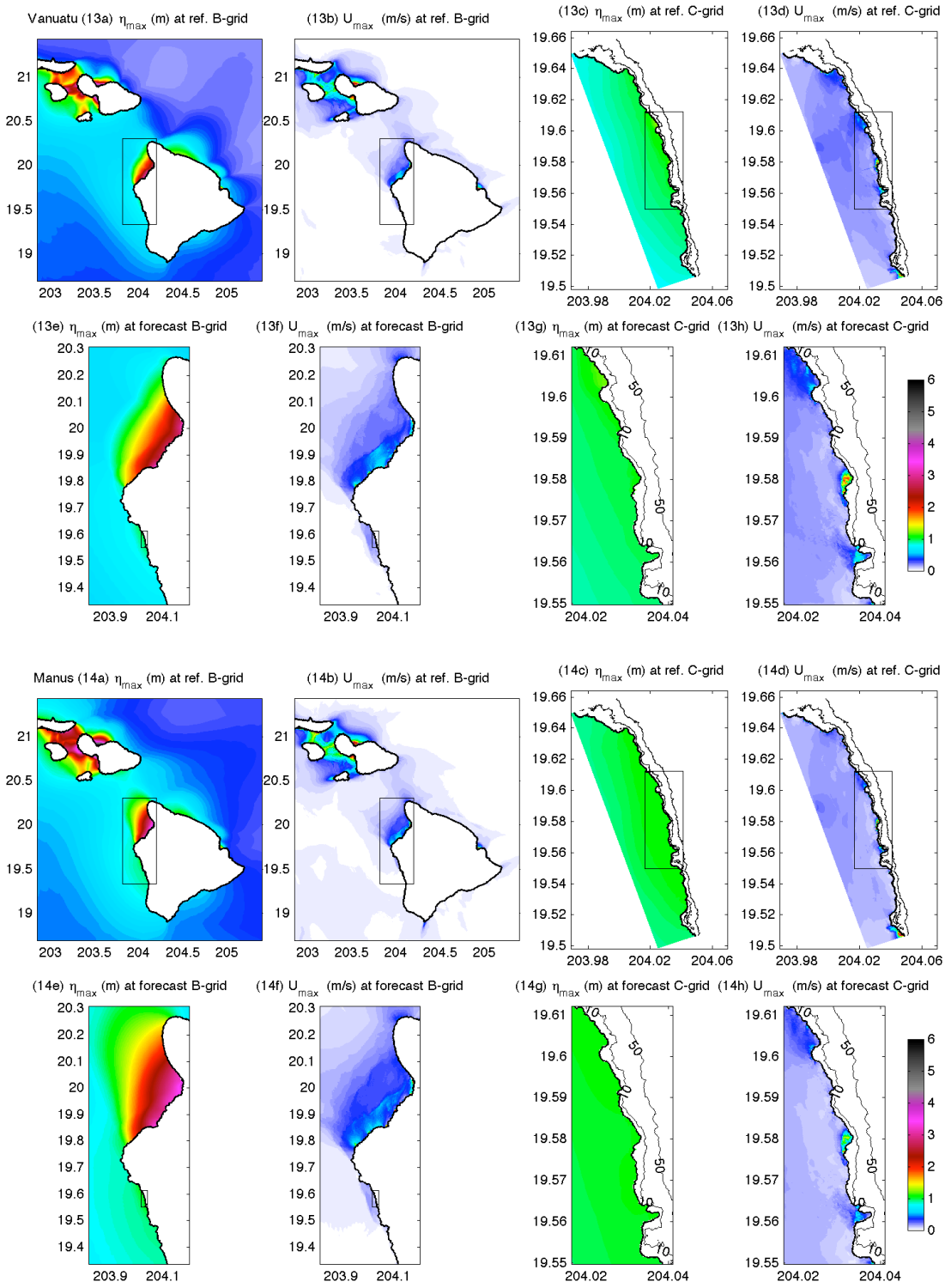
Vanuatu (13a) η_{max} (m) at ref. B-grid
(13b) U_{max} (m/s) at ref. B-grid
(13c) η_{max} (m) at ref. C-grid
(13d) U_{max} (m/s) at ref. C-grid
(13e) η_{max} (m) at forecast B-grid
(13f) U_{max} (m/s) at forecast B-grid
(13g) η_{max} (m) at forecast C-grid
(13h) U_{max} (m/s) at forecast C-grid
Manus (14a) η_{max} (m) at ref. B-grid
(14b) U_{max} (m/s) at ref. B-grid
(14c) η_{max} (m) at ref. C-grid
(14d) U_{max} (m/s) at ref. C-grid
(14e) η_{max} (m) at forecast B-grid
(14f) U_{max} (m/s) at forecast B-grid
(14g) η_{max} (m) at forecast C-grid
(14h) U_{max} (m/s) at forecast C-grid

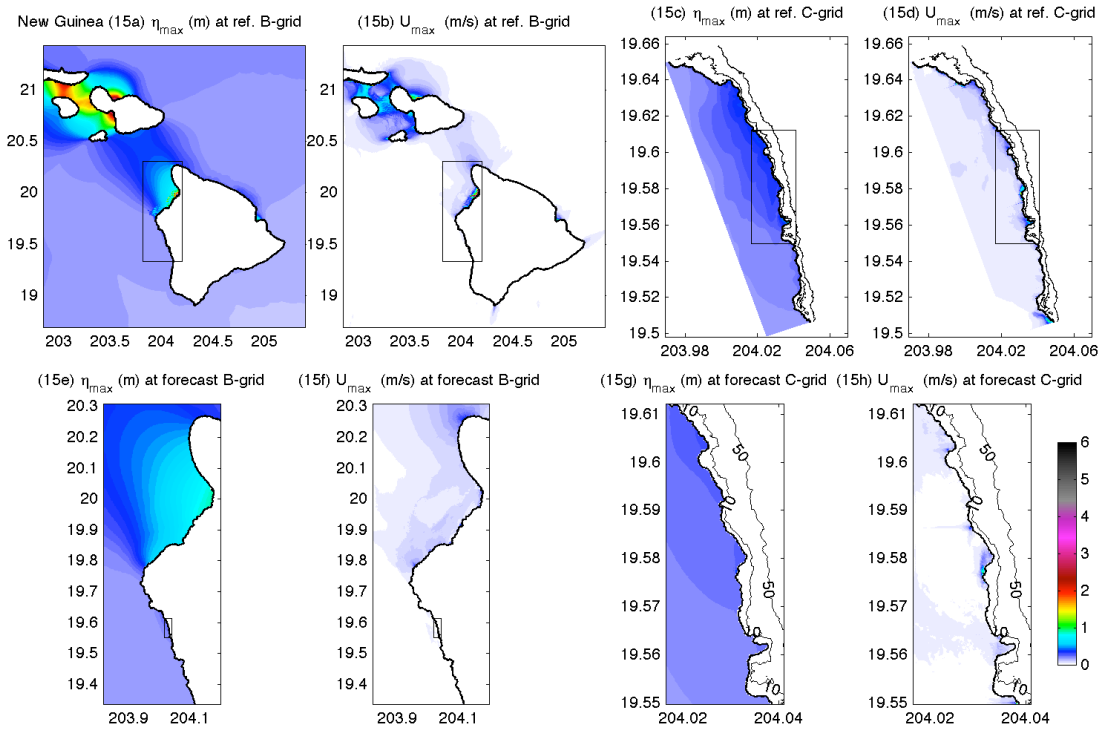
New Guinea (15a) η_{max} (m) at ref. B-grid
(15b) U_{max} (m/s) at ref. B-grid
(15c) η_{max} (m) at ref. C-grid
(15d) U_{max} (m/s) at ref. C-grid
(15e) η_{max} (m) at forecast B-grid
(15f) U_{max} (m/s) at forecast B-grid
(15g) η_{max} (m) at forecast C-grid
(15h) U_{max} (m/s) at forecast C-grid

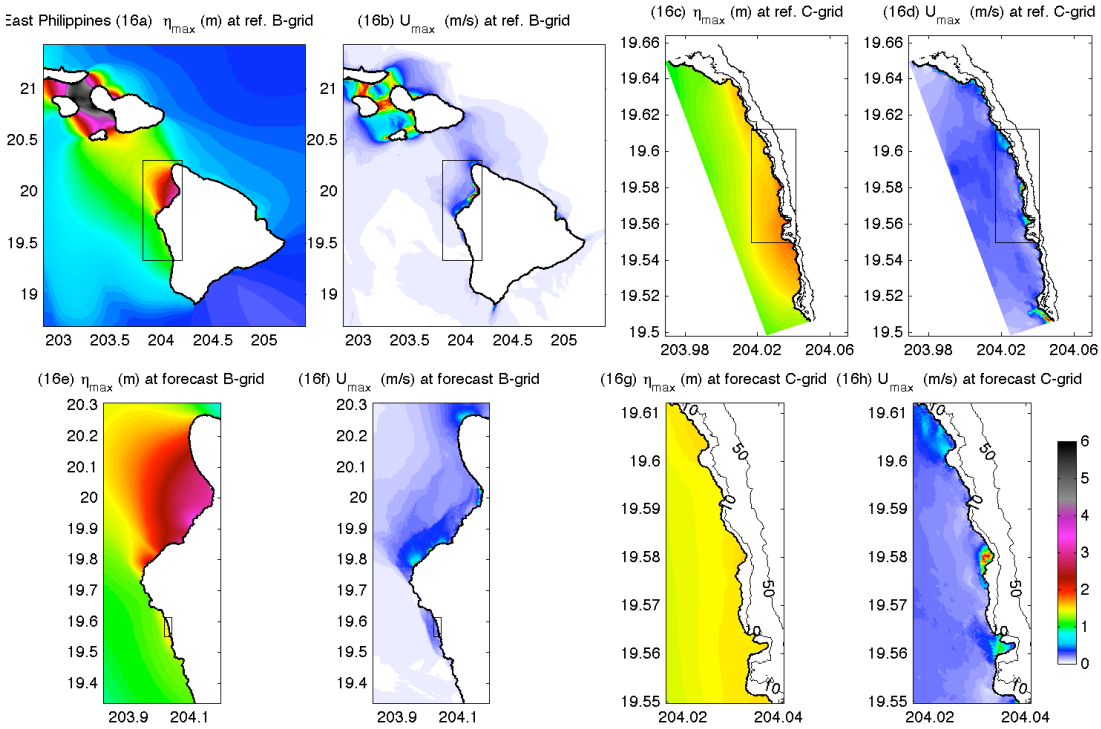
East Philippines (16a) η_{max} (m) at ref. B-grid
(16b) U_{max} (m/s) at ref. B-grid
(16c) η_{max} (m) at ref. C-grid
(16d) U_{max} (m/s) at ref. C-grid
(16e) η_{max} (m) at forecast B-grid
(16f) U_{max} (m/s) at forecast B-grid
(16g) η_{max} (m) at forecast C-grid
(16h) U_{max} (m/s) at forecast C-grid

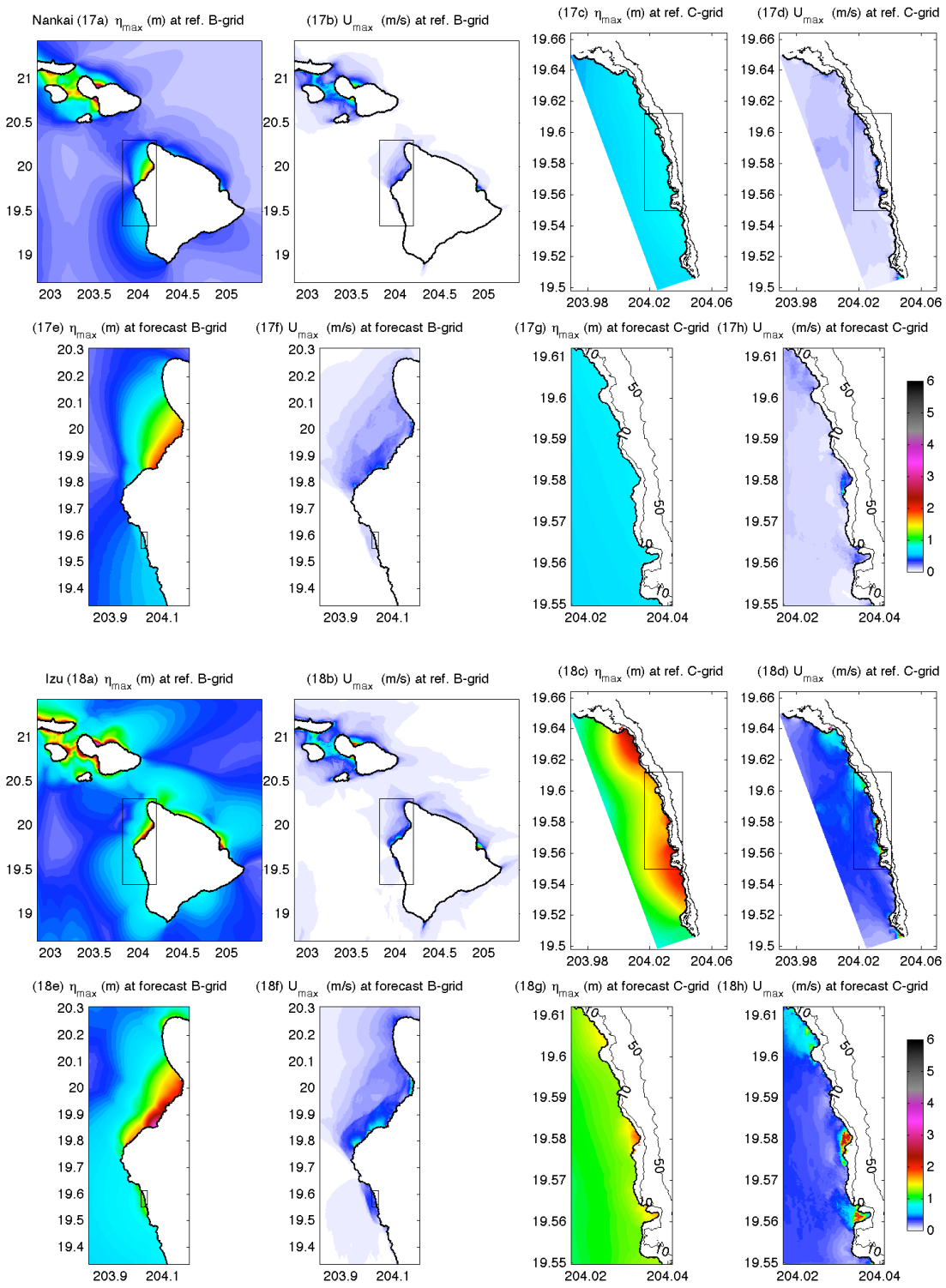

Figure 13 Computed maximum amplitude and current by the Keauhou (a, b, c and d) reference model and (e, f, g and h) forecast model for the eighteen simulated magnitude 9.3 tsunami.

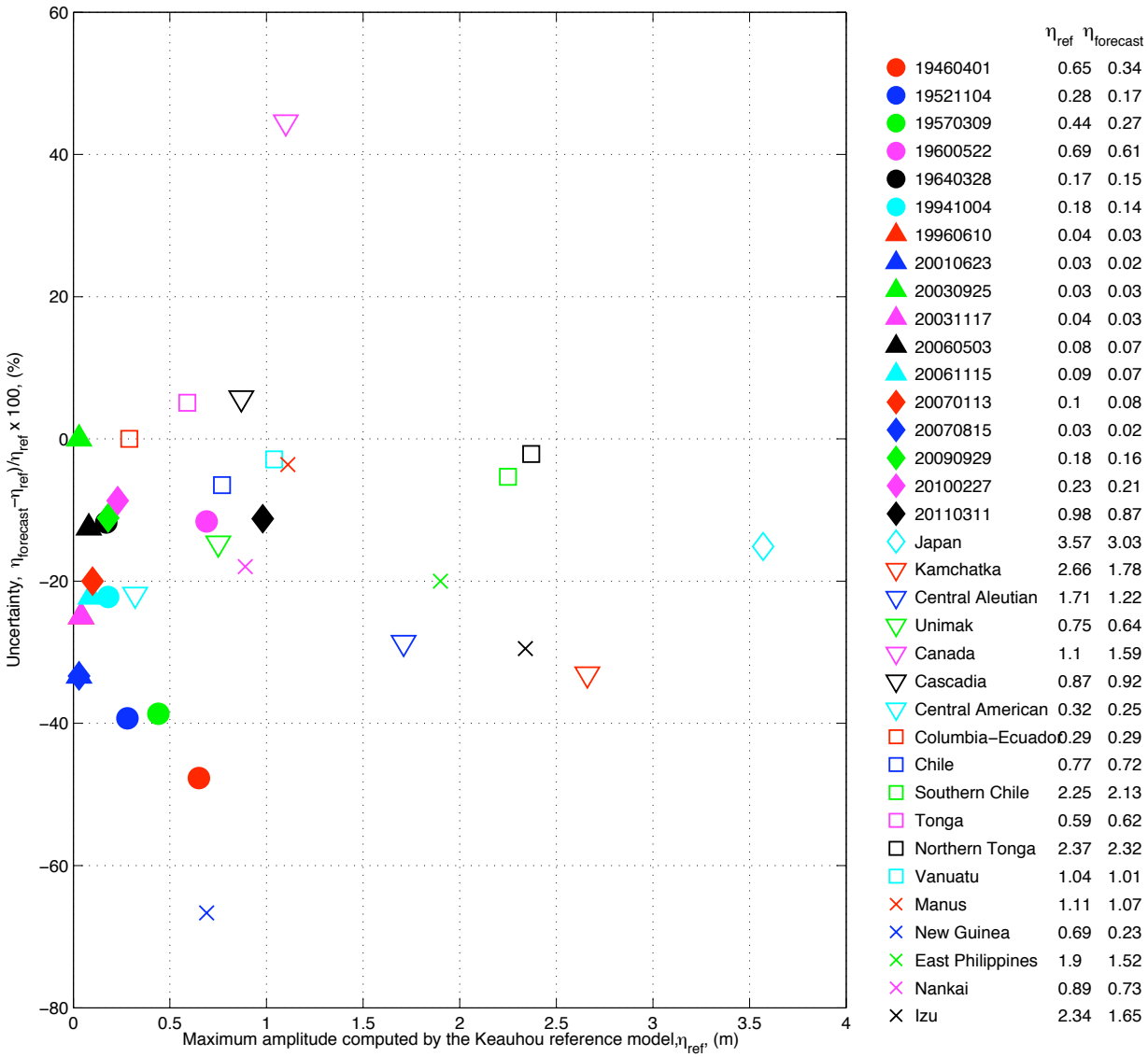

Figure 14 Maximum amplitude at Keauhou Warning point computed by the reference model and forecast model for 35 tsunamis. Filled markers, 17 past tsunamis; open markers, 18 magnitude 9.3 simulated tsunamis.